[American Journal of Science, Vol. 310, May, 2010, P. 364–404, DOI 10.2475/05.2010.02]

PERMIAN-TRIASSIC (260-220 MA) CRUSTAL GROWTH OF EASTERN CENTRAL ASIAN OROGENIC BELT AS REVEALED BY DETRITAL ZIRCON STUDIES

FANXUE MENG*,**,***, SHAN GAO**,***,†, HONGLIN YUAN***, and HUJUN GONG***

ABSTRACT. Present global compilations of ages and isotopic data suggest insignificant crustal growth after 450 Ma. Previous Nd isotopic studies of whole rocks from the Central Asian Orogenic Belt suggest large volumes of juvenile crustal additions in the Phanerozoic. To test this, we studied detrital zircons from the Xinglonggou Formation of western Liaoning at the northern margin of the North China craton, which was deposited after the collision between the Siberian Plate and the North China craton to form this part of the Central Asian Orogenic Belt. Zircons from the Xinglonggou sandstones are characterized by two major groups of U-Pb ages (2.6-2.4 Ga and 260-220 Ma) except for three grains (1.9-1.6 Ga). The 2.6 to 2.4 Ga zircons have positive ε_{Hf} (t) values up to coeval depleted mantle value, which suggest juvenile crustal addition. The results are consistent with existing data for the North China craton (NCC). ε_{Hf} (t) values of 260 to 220 Ma zircons range widely from −15.4 to 13.3. While zircons with the negative ε_{Hf} (t) values are similar to igneous zircons from intrusive rocks of the North China craton and indicate recycling of ancient continental crustal materials, those with the positive values and young model ages point to a significant period of crustal generation with the source provenance from the eastern Central Asian Orogenic Belt (CAOB) to the north. Mixing of detritus from both the North China craton and the eastern Central Asian Orogenic Belt suggests the ca. 250 Ma closure of the Paleo-Asian ocean and collision between the North China craton and the Siberian Plate along the eastern Solonker zone. The youngest zircons constrain uplift of the eastern Central Asian Orogenic Belt to be no older than 208 Ma. Thus, the 260 to 220 Ma crustal growth is related to the subduction of the Paleo-Asian ocean Plate along the Solonker suture, which records the termination of the Central Asian Orogenic Belt. The Solonker suture occupies an area of 700 km long and 60 km wide and extends from Solonker via Sonid Yuoqi to Linxi in Inner Mongolia and further west and northeast. This implies extensive juvenile crustal additions during this period. It may change our present views of Phanerozoic crustal growth.

Key words: Detrital zircon, U-Pb age, Hf isotope, North China craton, Crustal growth.

INTRODUCTION

Clastic sediments and sedimentary rocks are ideal samples for studying formation, evolution, and chemical composition of the continental crust (for example, Goldschmidt, 1933; Taylor and others, 1983; Taylor and McLennan, 1985; McLennan, 2001; Rudnick and Gao, 2003; Kemp and others, 2006; Hu and Gao, 2008; Hawkesworth and others, 2010). Detrital zircon is providing the most valuable information for this purpose, because its robust chemical and physical properties allows it to survive later disturbances and different growth zones within zircon crystals can be dated by U-Pb

* Graduate School, China University of Geosciences, N. 388 Lumo Road, Wuhan 430074, China
** State Key Laboratory of Geological Processes and Mineral Resources, China University of Geosciences, Wuhan 430074, China
*** State Key Laboratory of Continental Dynamics, Department of Geology, Northwest University, Xi'an 710069, China
† Corresponding author: Tel.: +86 27 67884940; fax: +86 27 67885096; E-mail address: sgao@263.net (Shan Gao)

isotopes, while their trace elements and Lu-Hf and O isotopic compositions provide an exceptional record of magmatic, and thus continental crustal evolution (Griffin and others, 2004; Condie and others, 2005, 2009; Iizuka and others, 2005; Veevers and others, 2005; Hawkesworth and Kemp, 2006a, 2006b; Coogan and Hinton, 2006; Kemp and others, 2006; Weislogel and others, 2006; Campbell and Allen, 2008; Yang and others, 2009; Hawkesworth and others, 2010). The zircon thermometer adds additional important information on the formation and evolution of the continental crust (Watson and Harrison, 2005; Watson and others, 2006; Ferry and Watson, 2007).

It has been estimated that >50 percent volume of the present continental crust formed by 2.5 Ga and >90 percent by 540 Ma (Taylor and McLennan, 1995; Hawkesworth and Kemp, 2006a). Worldwide compilations of zircon ages from juvenile crust indicate striking age peaks around 2.7 Ga, 1.9 Ga and 1.2 Ga, which suggest episodic rapid continental growth during thermal pulses associated with emplacement of mantle plumes (Condie, 1998, 2000). Post 1.2 Ga zircons show no such significant age peaks. Recent compilations of zircon ages of worldwide granitoids reveal seven igneous age peaks (3300, 2700, 2680, 2500, 2100, 1900 and 1100 Ma) (Condie and others, 2009). Nd isotope distributions of granitoids suggest important additions of juvenile continental crust at 2700, 2500, 2120, 1900, 1700, 1650, 800, 570 and 450 Ma (Condie and others, 2009). These compilations do not suggest significant crustal growth after 450 Ma.

There are cases of classic orogenic belts (Caledonides, Hercynides, Canadian Cordillera, Lachlan and New England Foldbelts, Central Asian Orogenic belts) where Phanerozoic crustal growth is considered to be significant based on positive ε_{Nd} (t) of granitoids (Jahn and others, 2000a, 2000b; Wu and others, 2000). However, *in-situ* determinations of U-Pb ages, Hf and oxygen isotopes of detrital zircons from the Lachlan Fold Belt of southeastern Australia reveal two prominent linear arrays that intersect the depleted mantle growth curve near 1.9 and 3.3 Ga ago (Kemp and others, 2006). The data indicate that crustal generation in part of Gondwana was limited to major pulses at 1.9 and 3.3 Ga, and the Phanerozoic zircons crystallized during repeated reworking of crust formed at these times. These results highlight the importance of *in-situ* zircon isotopic studies compared to whole-rock analysis, which may be compromised by mixing processes.

The Central Asian Orogenic Belt (CAOB) occupies a vast area that extends >5000 km from west to east and 1000 to 2000 km wide situated between the Siberian craton and North China. Previous Nd isotopic studies of whole rocks from the Central Asian Orogenic Belt suggest significant juvenile crustal additions in the Phanerozoic (500-120 Ma) (for example, Zonenshain and others, 1990; Sengör and others, 1993; Sengör and Natal'in, 1996; Jahn and others, 2000a, 2000b; 2004; Windley and others, 2007). The crustal growth was thought to be related to subduction-accretion with punctuated collision events between accreted blocks (Mossakovsky and others, 1994; Wu and others, 2000; Buchan and others, 2001; Hong and others, 2004; Helo and others, 2006; Jian and others, 2008). To test the large volume of Phanerozoic crustal growth in the Central Asian Orogenic Belt, we analyzed U-Pb ages and Hf isotopic compositions of detrital zircons from the Xinglonggou Formation in western Liaoning, which is located in the northern part of the North China craton (NCC). The North China craton collided with the Siberian Plate along the Central Asian Orogenic Belt. The Xinglonggou sandstones were deposited after the collision and thus provide clues to the sources of the Central Asian Orogenic Belt and the North China craton.

GEOLOGICAL SETTINGS AND SAMPLES

The Central Asian Orogenic Belt extends from the Urals Mts. via Kazakhstan, Kyrgyzstan, northwestern China, Mongolia and southern Siberia to the Okhotsk Sea in the Russian Far East (Zonenshain and others, 1990; Sengör and others, 1993; Mossakovsky and others, 1994; Yakubchuk and others, 2001; Yakubchuk, 2002). It is sandwiched between the Siberian craton in the north and the North China and Tarim cratons in the south (fig. 1A). It is composed of a variety of tectonic units, including Precambrian micro-continental blocks, ancient island arcs, ocean islands, accretionary complexes, ophiolites and passive continental margins. The amalgamation of these terranes occurred at various times in the Paleozoic and Mesozoic and was accompanied by episodes of magmatism, ranging in age from Ordovician (ca. 450 Ma) to Triassic-Cretaceous (ca. 220-120 Ma) that resulted in the emplacement of large volumes of granitoid intrusions (Jahn, 2004) and mafic volcanic rocks (Zhu and others, 2005), accompanied by lesser volumes of mafic-ultramafic rocks (Pirajno and others, 2008). Its growth began at ca. 1.0 Ga (Khain and others, 2002) and continued to ca. 250 Ma, when the Paleo-Asian ocean closed (Xiao and others, 2003).

The Solonker zone (fig. 1B) has been widely regarded as the site of final closure of the Paleo-Asian ocean (Tang, 1990; Sengör and others, 1993; Xiao and others, 2003; Wu and others, 2007; Chen and others, 2009). However, there is still much controversy concerning the timing of suturing. Some workers proposed that suturing took place during the Permian to early Triassic (300-230 Ma) (Sengör and others, 1993; Chen and others, 2000, 2009; Xiao and others, 2003; Wu and others, 2007; Jian and others, 2010); some preferred suturing during either the middle Devonian (Tang, 1990) or late Devonian to early Carboniferous (400-320 Ma) (Shao, 1991; Hong and others, 1995; Xu and Chen, 1997); others advocated a middle Mesozoic (130-110 Ma) suturing based on a controversial amphibolite $^{40}Ar/^{39}Ar$ age (Nozaka and Liu, 2002). The southern accretionary zone between the North China craton and the Solonker suture is characterized by the Mid-Ordovician-Early Silurian (ca. 488-438 Ma) (Jian and others, 2008) Ulan island arc-Ondor Sum subduction-accretion complex and the Bainaimiao arc (fig. 1B). This zone was consolidated by the Carboniferous-Permian when it evolved into an Andean-type magmatic margin above a south dipping subduction zone. The northern accretionary zone north of the Solonker suture extends southward from a Devonian to Carboniferous active continental margin, through the Hegenshan ophiolite arc accretionary complex to the Late Carboniferous (~310 Ma) (Chen and others, 2009) Baolidao arc associated with some accreted Precambrian blocks. This northern zone had consolidated by the Permian when it developed into an Andean-type magmatic margin above a north dipping subduction zone. Final subduction of the Paleo-Asian ocean caused the two opposing active continental margins to collide, leading to formation of the Solonker suture in the end-Permian (ca. 250 Ma) (Xiao and others, 2003).

The Central Asian Orogenic Belt is celebrated for its massive juvenile crustal production in the Phanerozoic (for example, Jahn and others, 2000a, 2000b). This is evidenced by the emplacement of voluminous granitoids of 500 to 120 Ma in age with low initial Sr isotopic ratios, generally positive ε_{Nd} (t) values and young Nd model ages (Shao and others, 1999; Chen and others, 2000; Jahn and others, 2000a, 2000b; Wu and others, 2000, 2002, 2003b, 2007). It should be noted that all these studies are based on whole-rock data, which may be compromised by mixing processes. For example, the whole rock Nd model ages range from 1028 to 645 Ma with an average of 764 Ma (Wu and others, 2003b), which are remarkably older than the age of magma and imply mixing with older crust if the Phanerozoic magma represented juvenile additions from the mantle. However, this is unclear. Two gigantic magmatic belts can be recognized in the Central Asian Orogenic Belt: a northern belt from central-northern Mongolia to Russian Transbaikalia and a southern belt from Kazakhstan through northern Xinjiang (NW China), southern Mongolia, to northeastern China (Chen and Arakawa, 2005).

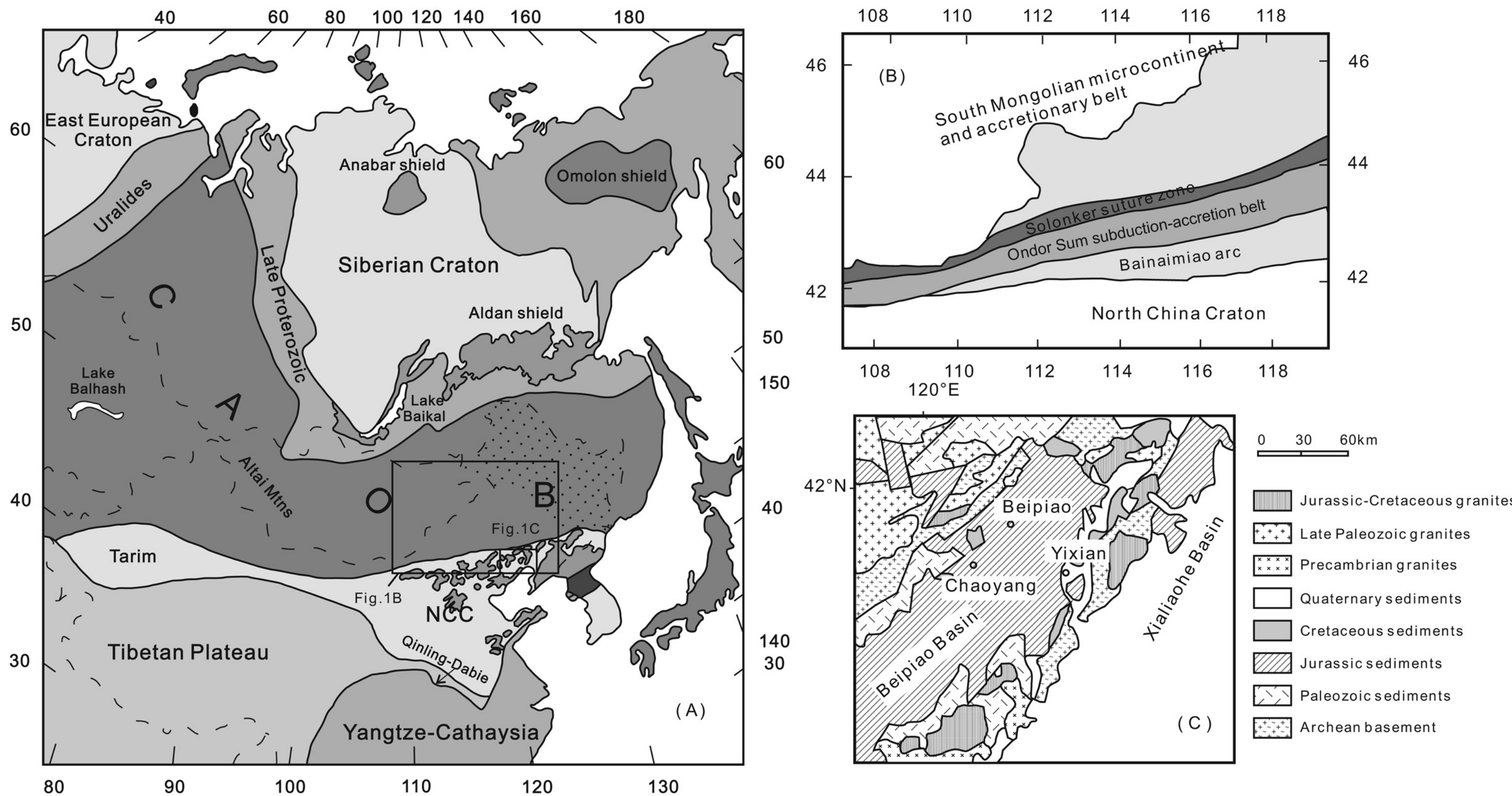

Fig. 1. (A) Simplified tectonic divisions of Central Asian Orogenic Belt (CAOB) (after Kröner and others, 2008), which is situated between the Siberian craton in the north and the North China (NCC) and Tarim cratons in the south. The dot area indicates drainage basins of rivers sampled for detrital zircon studies (Li, ms, 2010); (B) sketch map of Solonker suture zone (after Chen and others, 2009); (C) geologic map of western Liaoning Province (after Yan and others, 2006).

Previous studies of ophiolites and post-collision intrusive rocks suggest a west-east younging trend of a scissor-like closure of the Mongol-Okhotsk ocean (Donskaya and others, 2008). This is also true for the southern belt. In the western Central Asian Orogenic Belt (including Altai, Tianshan, and Kazakhstan), the closure occurred in the Late Carboniferous according to the ages of ophiolites and arc lavas (for example, Xu and others, 2006; Kröner and others, 2008), while the post-collision intrusive rocks mainly produced at 300 to 280 Ma, indicating a post-collisional environment in the Permian (for example, Han and others, 1997; Chen and Jahn, 2004; Wang and others, 2005, 2009). For example, in northern Xinjiang, post-collision granites were emplaced at about 340 to 265 Ma (Chen and Jahn, 2004; Chen and Arakawa, 2005; Wang and others, 2005; Han and others, 2006; Liu and Pan, 2006; Tong and others, 2006; Konopelko and others, 2007; Zhao and others, 2008; Zhou and others, 2008). However, the final closure of the Paleo-Asian ocean in the eastern Central Asian Orogenic Belt (including Inner Mongolia and northeastern China) occurred in the Permian-Triassic (296-230 Ma), which produced the Solonker suture (Sengör and others, 1993; Chen and others, 2009; Xiao and others, 2003). The ophiolites were dated at 299 to 284 Ma (Jian and others, 2008, 2010). Post-orogenic granitic rocks in Inner Mongolia were emplaced at ca. 280 Ma (Shi and others, 2004; Wang and others, 2004). In northeastern China, the existing age data indicate Phanerozoic granitic emplacement took place mainly from the Late Paleozoic to Late Mesozoic, which focused on Late Permian (270-250 Ma), Late Triassic-Early Jurassic (230-180 Ma), Middle Jurassic (170-150 Ma) and Cretaceous (ca. 120 Ma) (Chen and others, 2000; Jahn and others, 2000a, 2000b, 2001, 2004; Fan and others, 2003; Shi and others, 2004; Wu and others, 2000, 2002, 2003a, 2004, 2007; Ge and others, 2005; Cheng and others, 2006). However, the ca. 120 Ma granites may be related to the subduction of the Pacific Plate.

The mechanisms of continental crustal growth in the Central Asian Orogenic Belt remain the subject of debate. Sengör and others (1993) suggested that the Central Asian Orogenic Belt grew by 5.3 million square kilometers during the Palaeozoic, with nearly half of this growth being derived from the mantle by subduction accretion and arc collision. This model is supported by the presence of ophiolites with ages ranging from Neoproterozoic to late Paleozoic (for example, Coleman, 1989; Gao and Klemd, 2003; Xiao and others, 2003; Liu and Pan, 2006) and occurrences of Paleozoic arc-type magmatic rocks (for example, Chen and others, 2000; Heinhorst and others, 2000; Hu and others, 2000). Conversely, many researchers argue that massive Phanerozoic Central Asian Orogenic Belt granitoids with positive ε_{Nd} values are A-type granites generated by extensive basalt underplating in a post-orogenic or an intraplate extensional setting (for example, Zhao and others, 1996; Han and others, 1997; Jahn and others, 2000a, 2000b; Liu, 2002; Wu and others, 2000, 2002; Liu and Pan, 2006). It is also proposed that Late Paleozoic (~330 Ma) plume activity provided the heat required to generate the large amounts of granites and associated volcanic rocks in the Central Asian Orogenic Belt (Xia and others, 2004; Zhou and others, 2004).

The Yixian-Beipiao Basin of western Liaoning is located along the northern margin of the North China craton (fig. 1C). It is bounded by the eastern Central Asian Orogenic Belt to the north. Four major periods of volcanism have been identified in western Liaoning: the Jurassic Xinglonggou and Lanqi Formations, the Early Cretaceous Yixian Formation, and the late Early Cretaceous Zhanglaogongtun Formation (Yang and Li, 2008). The Xinglonggou Formation in this area represents the first sedimentation after the final collision of the eastern Central Asian Orogenic Belt with the North China craton. This formation is exposed in the Chaoyang-Beipiao area (fig. 1C) and variably overlies the Proterozoic Changcheng Group, the Middle Triassic strata or the Upper Triassic Laohugou Formation, and is overlain by the Beipiao Formation (Liu, ms, 2004). The Xinglonggou Formation consists of sandstones at the base and high-Mg adakite, andesite and dacite in the upper unit (Gao and others, 2004; Yan and others, 2006). Two sandstone samples XL130 and XL131 were taken from the base of the Xinglonggou Formation (fig. 2). They consist of 70 percent plagioclase, 15 percent quartz and 15 percent amphibole. Majority of the amphibole show the characteristics of alteration. The existence of amphibole and the high content plagioclase imply that they were derived from a near-by source. Zircons are typically prismatic or rounded to subhedral and lack of crack (fig. 3), which also suggests first cycle materials with short-distance of transportation.

ANALYTICAL METHODS

Samples of >10 kg were crushed and powdered. Zircons were separated by heavy-liquid and magnetic methods and then purified by hand picking under a binocular microscope. >2000 zircon grains were separated, from which >200 were selected and mounted on a double-sided tape, cast in epoxy resin, and polished to expose surfaces suitable for laser ablation inductively coupled plasma mass spectrometer (LA-ICP-MS) analysis. The surface of the grain mounts was acid-washed in dilute HNO_3 and pure ethanol to suppress lead contamination. As we are concerned with crustal growth related to magmatism, igneous zircons showing cathodoluminescence (CL) images of oscillatory zoning (fig. 3) were selected for age dating and Hf isotopic analysis. Metamorphic zircons, if any, were not considered. In addition, igneous zircon domains selected are free of cracks and inclusions, as guided by transmitted and reflected light images. Otherwise, zircons for analysis were selected randomly.

CL Imaging

Cathodoluminescence images of zircons were carried out using Quanta 400FEG high resolution emission field environmental scanning electron microscope connected with an Oxford INCA350 energy dispersive system and a Gatan Mono CL3+ CL system at the State Key Laboratory of Continental Dynamics, Northwest University. The imaging conditions were 10 kv with a spot size of 6.7 nm and a working distance of 8.4 mm. The CL images were used to demonstrate the internal textures of zircons and to select optimum spot locations for U-Pb dating.

U-Pb Dating

Zircons were dated on an excimer (193 nm wave length) laser ablation inductively coupled plasma mass spectrometer (LA-ICP-MS) at the State Key Laboratory of Continental Dynamics, Northwest University. The ICP-MS used is Agilent 7500a. The GeoLas 200M laser-ablation system (MicroLas, Göttingen, Germany) was used for the laser ablation experiments. Helium was used as carrier gas. The used spot size and laser frequency were 30 μm and 10 Hz, respectively. The data acquisition mode was peak jumping (20 ms per isotope each cycle). Raw count rates were measured for ^{29}Si, ^{204}Pb, ^{206}Pb, ^{207}Pb, ^{208}Pb, ^{232}Th and ^{238}U. U, Th and Pb concentrations were calibrated by using ^{29}Si as an internal standard and NIST SRM 610 as the reference standard. Each analysis consists of 30s gas blank and 40s signal acquisition. High-purity argon was used in combination with a home-made helium filtration column composed of a 10 L 13× molecular sieve. This column has filtering performance similar to charcoal filters (Hirata and Nesbitt, 1995; Hirata and others, 2005) and gold traps (Storey and others, 2006). The gas purification reduces the gas backgrounds of ^{202}Hg from >800 counts per second (cps) to <200 cps and those of ^{208}Pb from >400 cps to <100 cps. These

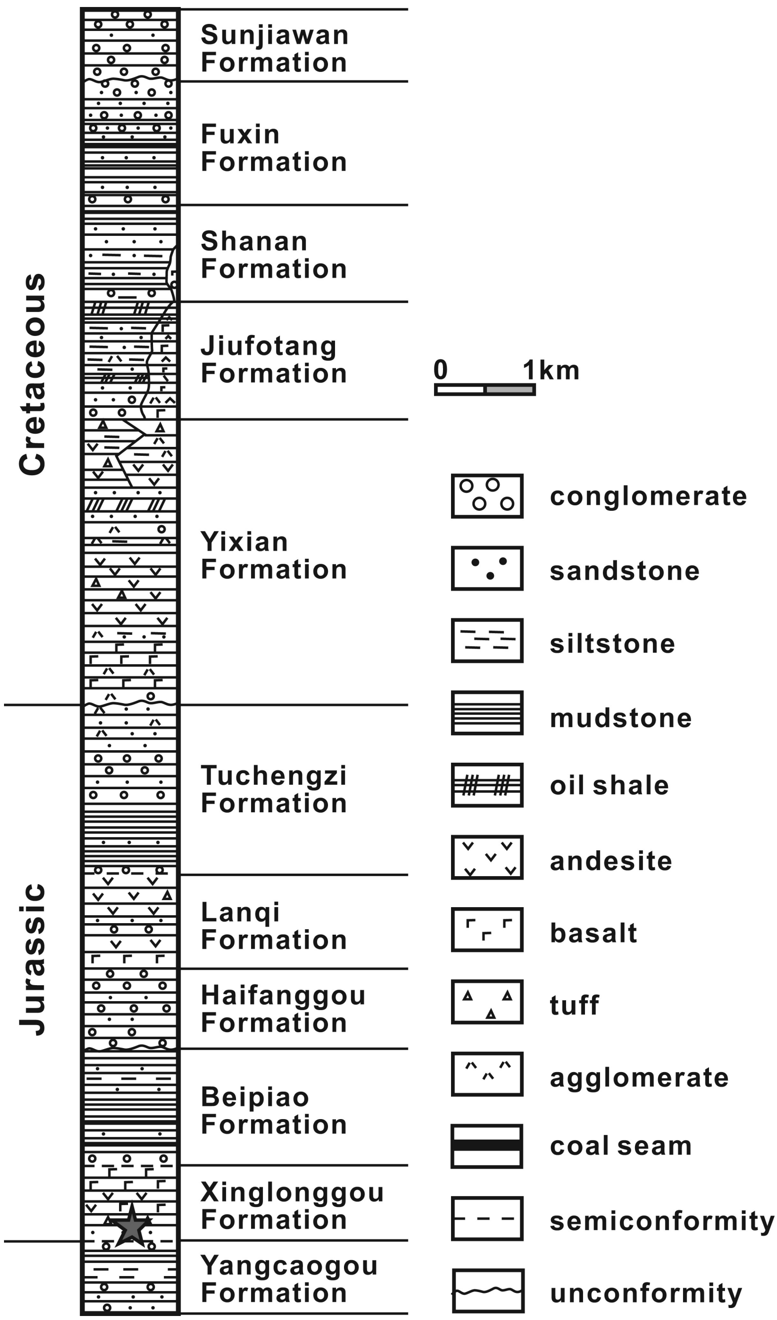

Fig. 2. Mesozoic stratigraphic column of western Liaoning (modified after Chen and others, 1997). Our samples are from the bottom of the Xinglonggou Formation at the south of Beipiao as represented by the star.

backgrounds were measured by ion counters (MC-ICPMS); they correspond to 0.05 and 0.1 parts per trillion (ppt) for ^{202}Hg and ^{208}Pb, respectively (Yuan and others, 2008). $^{207}Pb/^{206}Pb$, $^{206}Pb/^{238}U$, $^{207}Pb/^{235}U$ and $^{208}Pb/^{232}Th$ ratios, calculated using

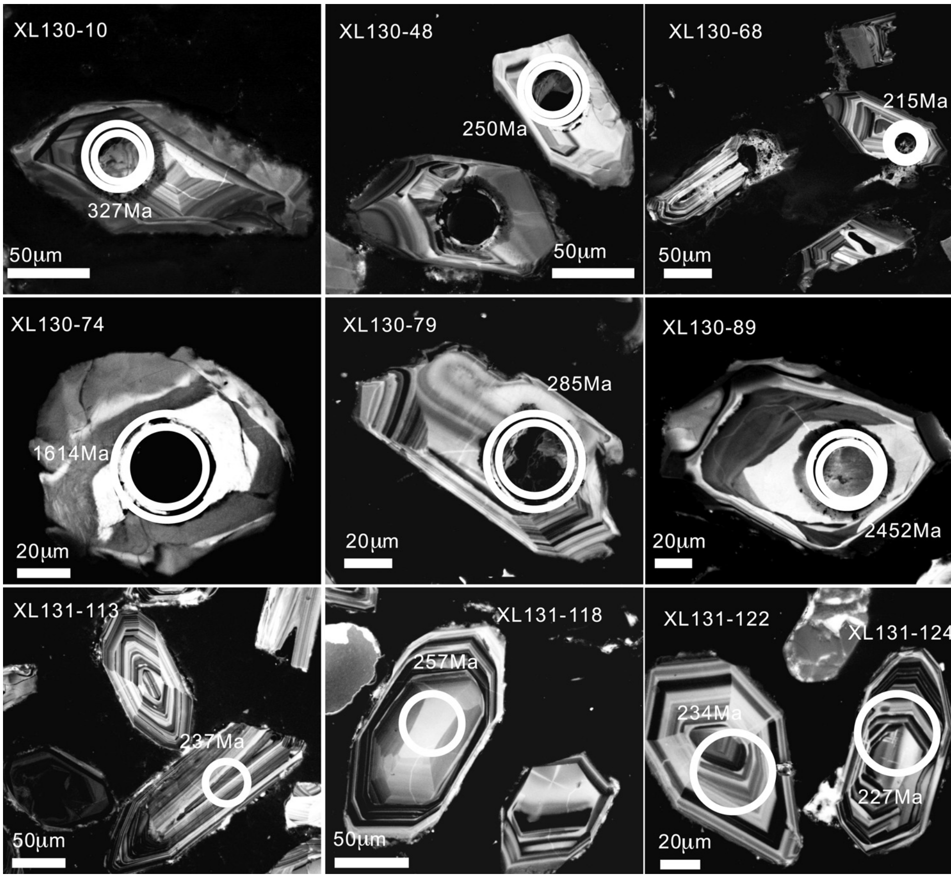

Fig. 3. Cathodoluminescence (CL) images of representative detrital zircons from the Xinglonggou Formation. For XL130, small and large circles indicate locations for U-Pb dating by LA-ICP-MS and *in-situ* Hf isotope analysis, respectively. Circles for XL131 indicate locations for simultaneous U-Pb and Hf isotope analysis. Numbers denote $^{207}Pb/^{206}Pb$ ages for zircons $\geq$1.0 Ga and $^{206}Pb/^{238}U$ ages for zircons <1.0Ga.

GLITTER 4.0 (Macquarie University), were corrected for both instrumental mass bias and depth-dependent elemental and isotopic fractionation using Harvard zircon 91500 as external standard. In data reduction, signals were selected to include the part as smooth and wide as possible with similar $^{206}Pb/^{238}U$ and $^{207}Pb/^{235}U$ ratios and signal spikes were eliminated. The ages were calculated using ISOPLOT 3 (Ludwig, 2003). Our measurements of GJ-1 (table 1) as an unknown yielded weighted $^{206}Pb/^{238}U$ ages of 603.2±1.0 Ma (2σ, MSWD=0.03, n=18) (fig. 4), which is in good agreement with the apparent ID-TIMS $^{206}Pb/^{238}U$ ages of 598.5 to 602.7 Ma (Jackson and others, 2004). Analytical details for age and trace and rare earth element determinations of zircons are reported in Yuan and others (2004). Common Pb corrections were made following the method of Andersen (2002). Because measured ^{204}Pb usually accounts for <0.3 percent of the total Pb, the correction is insignificant in most cases.

As shown by Vermeesch (2004), for provenance studies, a minimum of 117 detrital zircon grains have to be dated for a single sample in order to yield statistically significant results. A total of 121 zircons were dated for XL130 and 125 zircons for XL131.

TABLE 1

U-Pb isotopic data of zircon standard GJ-1

Analysis No.	Pb (ppm)	Th (ppm)	U (ppm)	isotopic ratios						Age (Ma)					
				$^{207}Pb/^{206}Pb$	1σ	$^{207}Pb/^{235}U$	1σ	$^{206}Pb/^{238}U$	1σ	$^{207}Pb/^{206}Pb$	1σ	$^{207}Pb/^{235}U$	1σ	$^{206}Pb/^{238}U$	1σ
JUN23A24	27	6.3	237	0.06053	0.00085	0.81746	0.00929	0.09794	0.00063	622.5	30.0	606.6	5.2	602.3	3.7
JUN23A46	26	6.1	226	0.06004	0.00091	0.81178	0.01027	0.09804	0.00065	605.2	32.4	603.4	5.8	602.9	3.8
JUN23A66	27	6.3	225	0.06020	0.00087	0.81445	0.00968	0.09811	0.00063	610.8	31.0	604.9	5.4	603.3	3.7
JUN23A88	26	5.6	218	0.05907	0.00097	0.79911	0.0112	0.09810	0.00066	569.8	35.2	596.3	6.3	603.2	3.9
JUN23A108	26	6.2	254	0.06077	0.00080	0.82189	0.00841	0.09806	0.00062	631.1	28.0	609.1	4.7	603.0	3.7
JUN23A130	26	6.5	246	0.06039	0.00078	0.81703	0.00815	0.09810	0.00062	617.5	27.6	606.4	4.6	603.3	3.6
JUN23A150	26	6.3	239	0.05847	0.00081	0.79173	0.00882	0.09819	0.00063	547.4	30.0	592.2	5.0	603.8	3.7
JUN23A173	26	6.3	235	0.06020	0.00093	0.81362	0.01056	0.09800	0.00065	610.8	33.0	604.5	5.9	602.7	3.8
20070715C002	25	10	231	0.05784	0.00118	0.78295	0.01474	0.09812	0.00083	523.6	44.3	587.2	8.4	603.4	4.9
20070715C024	26	11	241	0.05949	0.00126	0.80454	0.01578	0.09805	0.00085	585.0	45.3	599.4	8.9	603.0	5.0
20070715C046	26	11	244	0.06201	0.00122	0.83911	0.01514	0.09812	0.00083	674.5	41.5	618.7	8.4	603.4	4.9
20070715C068	27	13	255	0.06153	0.00132	0.83224	0.01662	0.09808	0.00086	657.9	45.5	614.9	9.2	603.1	5.1
20070715C090	27	12	254	0.05652	0.00156	0.76456	0.02013	0.09810	0.00094	472.0	60.4	576.6	11.6	603.3	5.5
20070715C112	26	11	243	0.06047	0.00118	0.81766	0.01468	0.09806	0.00083	620.5	41.6	606.7	8.2	603.0	4.9
20070715C134	24	10	227	0.05944	0.00126	0.80425	0.01588	0.09813	0.00086	583.4	45.5	599.2	8.9	603.4	5.0
20070715C156	25	10	234	0.06058	0.00125	0.81970	0.0157	0.09814	0.00085	624.4	44.0	607.9	8.8	603.5	5.0
20070715C172	26	11	241	0.05954	0.00134	0.80526	0.01687	0.09810	0.00088	586.8	48.0	599.8	9.5	603.3	5.2
20070715C188	26	11	246	0.05947	0.00147	0.80461	0.01879	0.09813	0.00092	584.4	52.9	599.4	10.6	603.5	5.4

Excel files of Tables 1–4 are available from the authors upon request.

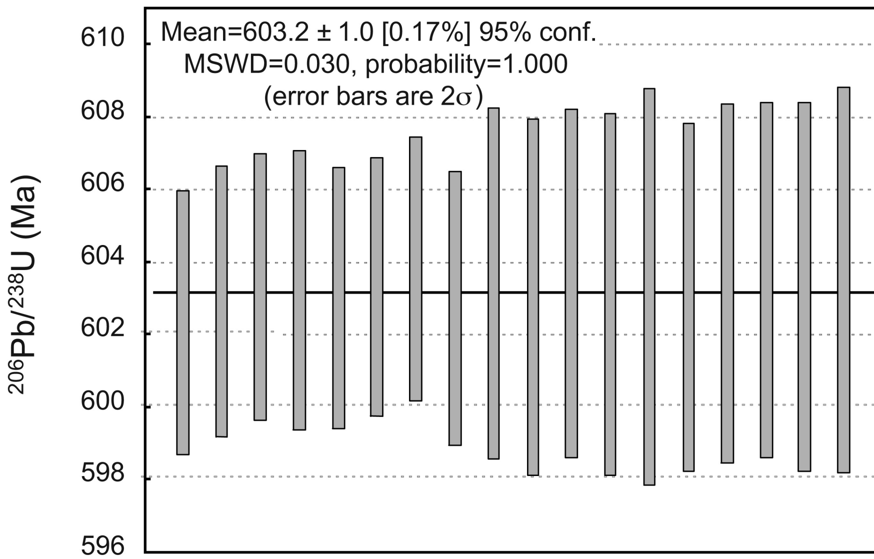

Fig. 4. Weighed mean age for zircon standard GJ-1.

Lu-Hf Isotope Analysis

Hf isotope analysis was done on a Nu Plasma HR MC-ICP-MS (Nu Instruments Ltd., UK), coupled to a GeoLas 2005 excimer ArF laser-ablation system hosted in the State Key Laboratory of Continental Dynamics, Northwest University. The energy density applied was 15–20 J/cm^2 and a spot size of 44 μm was used. Raw count rates for isotopes 171–177, 179, 180 and 182 were measured during a single data acquisition. Helium was also used as carrier gas. The sensitivity in laser ablation mode is 7–8 V per 1 percent of hafnium at 44 μm.

Isobaric interference corrections for ^{176}Lu and ^{176}Yb on ^{176}Hf must be determined precisely. The interference of ^{176}Lu on ^{176}Hf was corrected by measuring the intensity of ^{175}Lu and using the ^{176}Lu/^{175}Lu ratio of 0.02669 (De Bievre and Taylor, 1993) to correct the measured ^{176}Hf/^{177}Hf ratios. Similarly, the interference of ^{176}Yb on ^{176}Hf was corrected by measuring the interference-free ^{172}Yb isotope and using the recommended ^{176}Yb/^{172}Yb ratio of 0.5886 (Chu and others, 2002) to calculate ^{176}Hf/^{177}Hf ratios. In doing so, a mean ^{173}Yb/^{171}Yb ratio for the analyzed spot itself was automatically used in the same run to calculate a mean β_{Yb} value (Iizuka and Hirata, 2005), and then the ^{176}Yb signal intensity was calculated from the ^{173}Yb signal intensity and the mean β_{Yb} value.

The Hf isotopes were measured in two modes. For XL130, the analysis was done on the same spots or the same age domains for age determinations, as guided by CL images. For XL131, we used our developed technique of simultaneous determinations of U-Pb ages, Hf isotopes and trace element compositions of zircon by combining excimer laser ablation quadrupole and multiple collector ICP-MS (Yuan and others, 2008). This allows simultaneous collections of data on U-Pb age, Hf isotope and trace element composition of the same aerosol from the same spot of zircon. The similar Hf isotopic compositions obtained by the two modes of Hf analysis indicate that both modes of Hf analysis work and age zoning is not a problem for our zircons, which mostly do not show age zoning (fig. 3). Our measured values of three well-characterized zircon standards (91500, GJ-1 and MON-1) agree with the recom-

Table 2

Lu-Hf isotopic compositions of zircon standards

Sample	$^{176}Hf/^{177}Hf$	2σ	$^{176}Yb/^{177}Hf$	2σ	$^{176}Lu/^{177}Hf$	2σ
91500	0.282241	0.000048	0.009304	0.000032	0.000302	0.000001
91500	0.282274	0.000042	0.008901	0.000038	0.000297	0.000001
91500	0.282185	0.000042	0.009360	0.000120	0.000301	0.000001
91500	0.282368	0.000050	0.009117	0.000034	0.000302	0.000001
91500	0.282267	0.000056	0.009106	0.000102	0.000301	0.000001
91500	0.282360	0.000050	0.009146	0.000070	0.000308	0.000001
91500	0.282279	0.000048	0.009231	0.000046	0.000308	0.000001
91500	0.282371	0.000034	0.008847	0.000042	0.000298	0.000001
91500	0.282353	0.000058	0.008953	0.000080	0.000303	0.000001
91500	0.282454	0.000046	0.009348	0.000052	0.000305	0.000001
91500	0.282265	0.000038	0.009277	0.000050	0.000305	0.000001
91500	0.282276	0.000050	0.008987	0.000038	0.000299	0.000001
91500	0.282337	0.000052	0.009142	0.000118	0.000297	0.000001
91500	0.282241	0.000058	0.009234	0.000044	0.000304	0.000001
91500	0.282269	0.000054	0.009297	0.000042	0.000302	0.000001
91500	0.282281	0.000044	0.009502	0.000070	0.000304	0.000001
91500	0.282204	0.000048	0.009598	0.000038	0.000303	0.000001
91500	0.282186	0.000044	0.009441	0.000112	0.000306	0.000001
91500	0.282250	0.000048	0.009044	0.000034	0.000301	0.000001
91500	0.282469	0.000050	0.008983	0.000044	0.000301	0.000001
91500	0.282340	0.000054	0.009154	0.000048	0.000302	0.000001
91500	0.282413	0.000048	0.009177	0.000024	0.000299	0.000001
91500	0.282202	0.000044	0.009369	0.000076	0.000304	0.000001
91500	0.282287	0.000042	0.009183	0.000026	0.000300	0.000001
91500	0.282121	0.000042	0.009493	0.000120	0.000309	0.000005
91500	0.282178	0.000040	0.009151	0.000032	0.000303	0.000001
91500	0.282313	0.000036	0.006809	0.000034	0.000279	0.000000
91500	0.282300	0.000032	0.006827	0.000044	0.000278	0.000001
91500	0.282319	0.000034	0.006795	0.000050	0.000277	0.000000
91500	0.282325	0.000034	0.006946	0.000076	0.000276	0.000001
91500 Ave (n=30)	0.282291	0.000046	0.008891	0.000058	0.000299	0.000001
GJ-1	0.281996	0.000046	0.007901	0.000066	0.000263	0.000001
GJ-1	0.282044	0.000052	0.007899	0.000036	0.000263	0.000001
GJ-1	0.281980	0.000046	0.008217	0.000042	0.000269	0.000001
GJ-1	0.281991	0.000042	0.008756	0.000100	0.000285	0.000001
GJ-1	0.282037	0.000042	0.008384	0.000052	0.000273	0.000001
GJ-1	0.282065	0.000052	0.008089	0.000072	0.000263	0.000001
GJ-1	0.281978	0.000054	0.007727	0.000080	0.000252	0.000001
GJ-1	0.282084	0.000046	0.007769	0.000042	0.000252	0.000001
GJ-1	0.282016	0.000046	0.008163	0.000062	0.000262	0.000001
GJ-1	0.282049	0.000048	0.008140	0.000074	0.000260	0.000001
GJ-1	0.281998	0.000040	0.005865	0.000044	0.000244	0.000000
GJ-1	0.281976	0.000032	0.005851	0.000042	0.000244	0.000000
GJ-1	0.282085	0.000024	0.005792	0.000038	0.000243	0.000000
GJ-1	0.282061	0.000030	0.005884	0.000034	0.000246	0.000000
GJ-1 Ave (n=14)	0.282026	0.000043	0.007460	0.000056	0.000258	0.000001

TABLE 2

(continued)

Sample	$^{176}Hf/^{177}Hf$	2σ	$^{176}Yb/^{177}Hf$	2σ	$^{176}Lu/^{177}Hf$	2σ
MON-1	0.282732	0.000032	0.000431	0.000013	0.000012	0.000000
MON-1	0.282815	0.000036	0.000486	0.000036	0.000013	0.000000
MON-1	0.282766	0.000046	0.000606	0.000032	0.000017	0.000000
MON-1	0.282781	0.000028	0.000501	0.000016	0.000013	0.000000
MON-1	0.282675	0.000030	0.000628	0.000014	0.000015	0.000000
MON-1	0.282712	0.000034	0.000583	0.000015	0.000015	0.000000
MON-1	0.282774	0.000019	0.000494	0.000015	0.000013	0.000000
MON-1	0.282690	0.000034	0.000437	0.000019	0.000011	0.000000
MON-1	0.282722	0.000034	0.000503	0.000017	0.000013	0.000001
MON-1	0.282747	0.000040	0.000587	0.000019	0.000013	0.000000
MON-1	0.282746	0.000022	0.000407	0.000019	0.000013	0.000000
MON-1	0.282728	0.000017	0.000434	0.000007	0.000014	0.000000
MON-1	0.282722	0.000022	0.000409	0.000014	0.000013	0.000000
MON-1	0.282714	0.000020	0.000410	0.000008	0.000013	0.000000
MON-1	0.282725	0.000026	0.000443	0.000009	0.000014	0.000000
MON-1	0.282709	0.000024	0.000431	0.000009	0.000013	0.000000
MON-1 Ave (n=16)	0.282735	0.000029	0.000487	0.000016	0.000013	0.000000

mended values to within 2σ (table 2). Detailed description of the technique and analyses of the six standard zircons (91500, Temora-2, GJ-1, Mud Tank, BR266 and Monastery) were reported in Yuan and others (2008).

The initial $^{176}Hf/^{177}Hf$ ratios were calculated with reference to the chondritic reservoir (CHUR) at the time of zircon growth from magmas. The decay constant for ^{176}Lu and the chondritic ratios of $^{176}Hf/^{177}Hf$ and $^{176}Lu/^{177}Hf$ used in calculations are 1.867×10^{-11} yr^{-1} (Scherer and others, 2001) and 0.282772 and 0.0332 (Bichert-Toft and Albarède, 1997), respectively. The two-stage continental model age (T_{DM2}) was calculated by projecting the initial $^{176}Hf/^{177}Hf$ of zircon back to the depleted mantle growth curve using $^{176}Lu/^{177}Hf = 0.0093$ for the upper continental crust (Vervoort and Patchett, 1996).

RESULTS

A total of 246 detrital zircons were dated, of which 180 are concordant with concordance within 90 to 110 percent. 149 concordant zircons were selected for Hf isotope analysis. Tables 3 and 4 give U-Pb and Hf data for the concordant zircons, respectively. Zircons are typically prismatic or rounded to subhedral. They are characterized by oscillatory zoning (fig. 3) and have Th/U ratios of >0.5 (fig. 5). These features indicate a magmatic origin and suggest first cycle materials with short-distance of transportation, which is supported by the presence of amphibole in the sandstones. The following discussion is confined to the concordant zircons. We use $^{207}Pb/^{206}Pb$ ages for zircons of age ≥1.0 Ga and $^{206}Pb/^{238}U$ ages for zircons of age <1.0 Ga.

U-Pb Ages

The two samples show similar bimodal age groups. 121 zircon grains were analyzed and 77 concordant ages were obtained on XL130. The concordant zircons show two major age populations: 255 to 220 Ma and 2600 to 2400 Ma (figs. 6 and 7). The obtained youngest age is 215±2 Ma (Spot XL130-068) and the oldest age is 2584±5 Ma (Spot XL130-100).

TABLE 3

U-Pb isotopic data of detrital zircons from sandstones in the Xinglonggou Formation, western Liaoning

Sample	Pb (ppm)	Th (ppm)	U (ppm)	isotopic ratios $^{207}Pb/^{206}Pb$	1σ	$^{207}Pb/^{235}U$	1σ	$^{206}Pb/^{238}U$	1σ	Age (Ma) $^{207}Pb/^{206}Pb$	1σ	$^{207}Pb/^{235}U$	1σ	$^{206}Pb/^{238}U$	1σ	Used age	Con%
XL130-02	95	73	164	0.16208	0.00168	10.24856	0.06768	0.45843	0.00282	2477	5	2457	6	2433	12	2477	101.81
XL130-04	21	146	380	0.05466	0.00098	0.34309	0.00572	0.04552	0.00029	399	41	300	4	287	2	287	104.53
XL130-05	11	71	226	0.0515	0.00089	0.30138	0.00454	0.04243	0.00029	263	22	267	4	268	2	268	99.63
XL130-06	19	124	405	0.05335	0.00076	0.29649	0.00341	0.04029	0.00026	344	15	264	3	255	2	255	103.53
XL130-07	7.6	68	166	0.05294	0.00104	0.28077	0.00494	0.03845	0.00027	326	27	251	4	243	2	243	103.29
XL130-08	47	38	91	0.14831	0.00161	8.29476	0.0606	0.40554	0.00256	2327	6	2264	7	2194	12	2327	106.06
XL130-10	3.0	56	40	0.04738	0.00157	0.34029	0.01072	0.05208	0.00048	68	54	297	8	327	3	327	90.83
XL130-11	21	24	34	0.15338	0.00188	9.04994	0.0841	0.42786	0.00299	2384	7	2343	8	2296	13	2384	103.83
XL130-15	8.9	231	144	0.05316	0.00123	0.26768	0.00567	0.03651	0.00028	336	34	241	5	231	2	231	104.33
XL130-18	13	174	248	0.05261	0.00089	0.28543	0.00416	0.03934	0.00026	312	21	255	3	249	2	249	102.41
XL130-19	4.5	43	85	0.05157	0.00131	0.28342	0.00671	0.03986	0.00032	266	39	253	5	252	2	252	100.40
XL130-20	7.9	132	135	0.05191	0.00107	0.28899	0.00541	0.04038	0.00029	281	30	258	4	255	2	255	101.18
XL130-21	7.7	110	137	0.05514	0.00128	0.30391	0.00647	0.03997	0.00031	418	34	269	5	253	2	253	106.32
XL130-22	12	149	247	0.05488	0.00109	0.26545	0.00472	0.03507	0.00025	407	27	239	4	222	2	222	107.66
XL130-23	12	196	236	0.05144	0.00097	0.24597	0.00413	0.03468	0.00024	261	26	223	3	220	1	220	101.36
XL130-24	89	328	1849	0.05232	0.00061	0.28372	0.00281	0.03933	0.00024	299	27	254	2	249	1	249	102.01
XL130-25	6.4	86	84	0.05398	0.00136	0.38577	0.00904	0.05183	0.00042	370	38	331	7	326	3	326	101.53
XL130-28	5.7	70	103	0.05301	0.00118	0.2916	0.00595	0.03989	0.0003	329	33	260	5	252	2	252	103.17
XL130-29	200	167	288	0.16219	0.00164	10.65067	0.06565	0.4762	0.00284	2479	5	2493	6	2511	12	2479	98.73
XL130-33	8.0	104	142	0.05351	0.00118	0.29148	0.00588	0.0395	0.00029	350	32	260	5	250	2	250	104.00
XL130-34	12	127	199	0.05682	0.00177	0.30834	0.00928	0.03936	0.00031	484	70	273	7	249	2	249	109.64
XL130-35	28	441	545	0.0512	0.0007	0.24639	0.00269	0.0349	0.00022	250	14	224	2	221	1	221	101.36
XL130-36	14	193	294	0.0537	0.0009	0.25493	0.00367	0.03443	0.00023	358	20	231	3	218	1	218	105.96
XL130-38	12	121	226	0.04807	0.00091	0.24914	0.00418	0.03758	0.00026	103	27	226	3	238	2	238	94.96
XL130-39	11	141	208	0.05423	0.00104	0.26939	0.00462	0.03603	0.00025	381	26	242	4	228	2	228	106.14
XL130-40	133	140	198	0.15862	0.00163	9.65857	0.06307	0.44158	0.00267	2441	5	2403	6	2358	12	2441	103.52
XL130-41	69	62	95	0.16235	0.00172	10.67576	0.07448	0.47685	0.00297	2480	5	2495	6	2514	13	2480	98.65
XL130-42	14	161	272	0.05566	0.00101	0.28956	0.0046	0.03773	0.00026	439	23	258	4	239	2	239	107.95
XL130-44	7.1	72	128	0.05596	0.00176	0.30199	0.00918	0.03914	0.00032	451	72	268	7	247	2	247	108.50
XL130-45	58	53	76	0.16929	0.00183	11.57848	0.08504	0.49599	0.00316	2551	6	2571	7	2597	14	2551	98.23
XL130-47	11	140	205	0.05275	0.00105	0.26747	0.00475	0.03677	0.00026	318	27	241	4	233	2	233	103.43
XL130-48	9.4	105	166	0.0494	0.00114	0.26888	0.00568	0.03947	0.0003	167	35	242	5	250	2	250	96.80
XL130-50	11	159	214	0.05541	0.00108	0.27566	0.0048	0.03608	0.00026	429	26	247	4	228	2	228	108.33

TABLE 3
(continued)

Sample	Pb (ppm)	Th (ppm)	U (ppm)	isotopic ratios $^{207}Pb/^{206}Pb$	1σ	$^{207}Pb/^{235}U$	1σ	$^{206}Pb/^{238}U$	1σ	Age (Ma) $^{207}Pb/^{206}Pb$	1σ	$^{207}Pb/^{235}U$	1σ	$^{206}Pb/^{238}U$	1σ	Used age	Con%
XL130-51	8.3	98	154	0.05116	0.00163	0.25649	0.00794	0.03636	0.00028	248	75	232	6	230	2	230	100.87
XL130-52	14	185	250	0.05146	0.00114	0.2627	0.00532	0.03702	0.00027	261	33	237	4	234	2	234	101.28
XL130-53	10	142	181	0.05374	0.00106	0.27088	0.0048	0.03655	0.00026	360	27	243	4	231	2	231	105.19
XL130-54	11	141	202	0.05112	0.00097	0.25683	0.00434	0.03644	0.00025	246	26	232	4	231	2	231	100.43
XL130-55	13	142	231	0.05239	0.00129	0.28319	0.0067	0.03921	0.00027	302	58	253	5	248	2	248	102.02
XL130-56	6.2	65	120	0.05315	0.00114	0.26654	0.00521	0.03636	0.00027	335	31	240	4	230	2	230	104.35
XL130-57	3.1	1.5	64	0.0507	0.00144	0.27424	0.0073	0.03922	0.00033	227	46	246	6	248	2	248	99.19
XL130-58	228	235	344	0.16289	0.00163	9.57044	0.05819	0.42606	0.00252	2486	5	2394	6	2288	11	2486	108.65
XL130-61	9.1	83	159	0.05132	0.00105	0.2853	0.00527	0.04031	0.00029	255	29	255	4	255	2	255	100.00
XL130-62	12	149	230	0.05161	0.00089	0.25232	0.0038	0.03545	0.00024	268	22	228	3	225	1	225	101.33
XL130-63	74	77	99	0.1563	0.00162	9.92956	0.06592	0.4607	0.0028	2416	5	2428	6	2443	12	2416	98.89
XL130-65	11	165	187	0.05453	0.00102	0.27985	0.00462	0.03721	0.00026	393	24	251	4	236	2	236	106.36
XL130-66	70	80	100	0.15297	0.00159	9.18725	0.06115	0.43551	0.00264	2379	5	2357	6	2331	12	2379	102.06
XL130-68	11	135	228	0.05477	0.00141	0.25607	0.0063	0.03391	0.00025	403	59	231	5	215	2	215	107.44
XL130-69	12	117	224	0.05303	0.00096	0.27813	0.0044	0.03803	0.00026	330	23	249	3	241	2	241	103.32
XL130-70	10	104	189	0.05487	0.00098	0.28166	0.0044	0.03722	0.00025	407	23	252	3	236	2	236	106.78
XL130-74	14	41	36	0.09946	0.00239	3.62029	0.08166	0.26399	0.00217	1614	46	1554	18	1510	11	1614	106.89
XL130-75	12	110	255	0.05434	0.00125	0.28591	0.00628	0.03816	0.00026	385	53	255	5	241	2	241	105.81
XL130-76	8.1	107	167	0.04996	0.00102	0.26767	0.00493	0.03884	0.00028	193	29	241	4	246	2	246	97.97
XL130-78	7.7	93	170	0.05108	0.00113	0.26036	0.00527	0.03696	0.00028	244	33	235	4	234	2	234	100.43
XL130-79	17	136	310	0.05757	0.00088	0.35954	0.00462	0.04528	0.0003	513	17	312	3	285	2	285	109.47
XL130-81	13	154	253	0.05482	0.00112	0.29407	0.0054	0.03889	0.00028	405	28	262	4	246	2	246	106.50
XL130-82	15	258	319	0.05031	0.00084	0.24527	0.00354	0.03535	0.00024	209	21	223	3	224	1	224	99.55
XL130-83	12	155	249	0.05564	0.00095	0.28861	0.00427	0.03761	0.00026	438	21	257	3	238	2	238	107.98
XL130-84	11	113	231	0.05263	0.0014	0.27798	0.00713	0.03831	0.00028	313	62	249	6	242	2	242	102.89
XL130-85	12	123	249	0.05234	0.00143	0.27403	0.00719	0.03797	0.00029	300	64	246	6	240	2	240	102.50
XL130-86	7.6	74	147	0.05213	0.00132	0.29999	0.00708	0.04173	0.00034	291	39	266	6	264	2	264	100.76
XL130-87	6.2	72	129	0.05004	0.00179	0.26779	0.00914	0.0388	0.00038	197	61	241	7	245	2	245	98.37
XL130-89	50	45	81	0.15965	0.0018	10.07577	0.08062	0.45762	0.00302	2452	6	2442	7	2429	13	2452	100.95
XL130-92	20	293	428	0.05284	0.00134	0.25493	0.00618	0.03499	0.00025	322	59	231	5	222	2	222	104.05
XL130-94	10	117	191	0.05711	0.00152	0.31474	0.00807	0.03997	0.00029	496	60	278	6	253	2	253	109.88
XL130-95	28	228	648	0.05514	0.00075	0.26913	0.00291	0.03539	0.00022	418	13	242	2	224	1	224	108.04
XL130-96	24	384	497	0.05382	0.00079	0.26625	0.00323	0.03587	0.00023	364	16	240	3	227	1	227	105.73
XL130-97	8.0	131	157	0.05465	0.00109	0.28188	0.00505	0.0374	0.00027	398	27	252	4	237	2	237	106.33

TABLE 3
(continued)

Sample	Pb (ppm)	Th (ppm)	U (ppm)	isotopic ratios $^{207}Pb/^{206}Pb$	1σ	$^{207}Pb/^{235}U$	1σ	$^{206}Pb/^{238}U$	1σ	Age (Ma) $^{207}Pb/^{206}Pb$	1σ	$^{207}Pb/^{235}U$	1σ	$^{206}Pb/^{238}U$	1σ	Used age	Con%
XL130-99	39	57	53	0.16417	0.00197	10.70148	0.09616	0.47267	0.0033	2499	7	2498	8	2495	14	2499	100.16
XL130-100	80	116	120	0.17271	0.00187	10.55242	0.07731	0.44303	0.00283	2584	5	2485	7	2364	13	2584	109.31
XL130-103	414	517	601	0.16401	0.00166	10.81623	0.06702	0.47822	0.00287	2497	5	2507	6	2520	13	2497	99.09
XL130-105	10	118	202	0.05524	0.00107	0.30088	0.00521	0.03949	0.00028	422	26	267	4	250	2	250	106.80
XL130-106	9.4	88	192	0.0523	0.00108	0.27793	0.00521	0.03853	0.00028	299	29	249	4	244	2	244	102.05
XL130-108	207	64	319	0.16336	0.00167	11.4205	0.07253	0.50695	0.00306	2491	5	2558	6	2644	13	2491	94.21
XL130-112	6.2	95	107	0.05511	0.00242	0.29986	0.01284	0.03946	0.00037	417	100	266	10	249	2	249	106.83
XL130-113	26	636	491	0.05337	0.00084	0.25758	0.0034	0.035	0.00023	345	18	233	3	222	1	222	104.95
XL130-115	12	137	241	0.05235	0.00091	0.26556	0.00403	0.03679	0.00025	301	22	239	3	233	2	233	102.58
XL130-119	20	298	378	0.05593	0.00169	0.26832	0.00788	0.03479	0.00024	450	69	241	6	220	2	220	109.55
XL131-001	7.8	125	149	0.04885	0.00193	0.26311	0.01001	0.03904	0.00044	141	68	237	8	247	3	247	95.95
XL131-002	8.4	150	174	0.04977	0.0026	0.24638	0.0125	0.03589	0.00049	184	92	224	10	227	3	227	98.68
XL131-003	23	83	587	0.05056	0.00108	0.24568	0.00486	0.03523	0.00029	221	30	223	4	223	2	223	100.00
XL131-004	35	965	656	0.05429	0.00225	0.25546	0.01032	0.03413	0.00032	383	95	231	8	216	2	216	106.94
XL131-005	62	97	81	0.15868	0.00198	11.01273	0.11548	0.50315	0.00415	2442	8	2524	10	2627	18	2442	96.75
XL131-006	71	958	1322	0.05482	0.00141	0.30939	0.00755	0.04093	0.00033	405	59	274	6	259	2	259	105.79
XL131-009	16	243	340	0.05052	0.00128	0.25683	0.00613	0.03686	0.00033	219	39	232	5	233	2	233	99.57
XL131-010	22	267	535	0.05293	0.00158	0.24649	0.007	0.03376	0.00033	326	47	224	6	214	2	214	104.67
XL131-011	8.4	102	179	0.0493	0.00202	0.25686	0.01015	0.03777	0.00043	162	71	232	8	239	3	239	97.07
XL131-012	17	249	387	0.04999	0.00133	0.23998	0.00604	0.0348	0.00032	195	41	218	5	221	2	221	98.64
XL131-013	21	331	440	0.05371	0.00177	0.26968	0.0085	0.0364	0.00038	359	52	242	7	230	2	230	105.22
XL131-014	16	177	346	0.05079	0.00164	0.2538	0.00783	0.03623	0.00036	231	53	230	6	229	2	229	100.44
XL131-015	8.6	100	187	0.05105	0.00226	0.26241	0.0112	0.03727	0.00046	243	76	237	9	236	3	236	100.42
XL131-017	11	197	228	0.0539	0.00202	0.26794	0.00964	0.03604	0.0004	367	61	241	8	228	2	228	105.70
XL131-020	15	357	284	0.05431	0.00223	0.26442	0.01044	0.0353	0.00042	384	67	238	8	224	3	224	106.25
XL131-021	11	160	226	0.04948	0.00157	0.26345	0.00798	0.03861	0.00038	171	52	237	6	244	2	244	97.13
XL131-022	12	158	262	0.05487	0.00169	0.28299	0.00831	0.03739	0.00037	407	48	253	7	237	2	237	106.75
XL131-023	10	115	215	0.05091	0.0023	0.2573	0.01121	0.03665	0.00045	237	78	232	9	232	3	232	100.00
XL131-024	8.0	90	171	0.0543	0.00264	0.28036	0.01319	0.03743	0.0005	384	82	251	10	237	3	237	105.91
XL131-026	13	181	267	0.05175	0.00178	0.26407	0.0087	0.037	0.00039	274	56	238	7	234	2	234	101.71
XL131-028	9.0	113	183	0.05131	0.00244	0.27327	0.01257	0.03861	0.0005	255	82	245	10	244	3	244	100.41
XL131-029	12	234	261	0.0487	0.00164	0.23515	0.0076	0.03501	0.00036	133	57	214	6	222	2	222	96.40
XL131-030	10	101	204	0.05012	0.00207	0.26829	0.01067	0.03881	0.00045	201	71	241	9	245	3	245	98.37
XL131-031	13	209	287	0.05139	0.00198	0.2507	0.00927	0.03537	0.00039	258	65	227	8	224	2	224	101.34

TABLE 3

(continued)

Sample	Pb	Th	U	isotopic ratios						Age (Ma)							
	(ppm)	(ppm)	(ppm)	$^{207}Pb/^{206}Pb$	1σ	$^{207}Pb/^{235}U$	1σ	$^{206}Pb/^{238}U$	1σ	$^{207}Pb/^{206}Pb$	1σ	$^{207}Pb/^{235}U$	1σ	$^{206}Pb/^{238}U$	1σ	Used age	Con%
XL131-032	11	182	265	0.05108	0.00275	0.23067	0.01213	0.03275	0.00038	244	125	211	10	208	2	208	101.44
XL131-033	7.9	71	162	0.0511	0.00292	0.27061	0.01508	0.03841	0.00047	245	132	243	12	243	3	243	100.00
XL131-034	15	237	327	0.05089	0.00153	0.25331	0.00727	0.03609	0.00035	236	48	229	6	229	2	229	100.00
XL131-035	5.9	62	122	0.05133	0.00216	0.2745	0.01113	0.03878	0.00046	256	71	246	9	245	3	245	100.41
XL131-036	8.1	107	178	0.05005	0.00179	0.24817	0.00852	0.03595	0.00038	197	60	225	7	228	2	228	98.68
XL131-037	4.4	40	85	0.05168	0.00248	0.29558	0.01374	0.04147	0.00054	271	83	263	11	262	3	262	100.38
XL131-038	10	139	220	0.05134	0.0017	0.25384	0.00802	0.03585	0.00037	256	54	230	6	227	2	227	101.32
XL131-039	9.4	107	212	0.05596	0.00306	0.25792	0.01379	0.03343	0.0004	451	125	233	11	212	2	212	109.91
XL131-041	9.2	108	185	0.05374	0.00289	0.2916	0.01519	0.03934	0.00057	360	91	260	12	249	4	249	104.42
XL131-042	6.4	87	146	0.05586	0.00364	0.26886	0.01698	0.0349	0.0006	447	110	242	14	221	4	221	109.50
XL131-044	13	150	288	0.04963	0.00164	0.25302	0.008	0.03697	0.00037	178	55	229	6	234	2	234	97.86
XL131-045	37	73	94	0.10909	0.00166	4.27995	0.05734	0.28449	0.00243	1784	13	1690	11	1614	12	1784	105.56
XL131-047	17	337	339	0.05111	0.0017	0.25615	0.00818	0.03634	0.00037	246	55	232	7	230	2	230	100.87
XL131-048	13	177	270	0.05124	0.00155	0.26722	0.00773	0.03782	0.00037	252	48	240	6	239	2	239	100.42
XL131-049	16	213	343	0.05128	0.00138	0.25916	0.00662	0.03664	0.00034	253	42	234	5	232	2	232	100.86
XL131-052	24	539	414	0.05149	0.00208	0.2761	0.01072	0.03888	0.00045	263	68	248	9	246	3	246	100.81
XL131-053	8.6	99	188	0.05056	0.00189	0.25641	0.00922	0.03678	0.0004	221	63	232	7	233	2	233	99.57
XL131-054	15	199	292	0.05205	0.00254	0.25693	0.01227	0.0358	0.00036	288	114	232	10	227	2	227	102.20
XL131-055	13	170	268	0.051	0.00166	0.25988	0.00808	0.03695	0.00037	241	53	235	7	234	2	234	100.43
XL131-056	41	282	862	0.05137	0.00095	0.28747	0.00482	0.04058	0.00032	257	24	257	4	256	2	256	100.39
XL131-057	12	158	265	0.05105	0.00184	0.25801	0.00891	0.03665	0.00039	243	60	233	7	232	2	232	100.43
XL131-058	12	141	254	0.05007	0.00169	0.25516	0.00824	0.03696	0.00038	198	56	231	7	234	2	234	98.72
XL131-059	6.7	103	145	0.05124	0.00222	0.25244	0.01054	0.03573	0.00043	252	74	229	9	226	3	226	101.33
XL131-060	15	161	322	0.05135	0.00144	0.26809	0.00711	0.03786	0.00035	257	44	241	6	240	2	240	100.42
XL131-061	7.4	100	159	0.05458	0.00228	0.27804	0.01117	0.03694	0.00044	395	69	249	9	234	3	234	106.41
XL131-062	14	267	259	0.05251	0.00197	0.28763	0.01038	0.03973	0.00044	308	62	257	8	251	3	251	102.39
XL131-063	79	106	119	0.15724	0.002	10.14522	0.10902	0.46792	0.0039	2426	8	2448	10	2474	17	2426	99.10
XL131-064	18	260	382	0.05428	0.00149	0.27855	0.00725	0.03721	0.00035	383	41	250	6	236	2	236	105.93
XL131-065	2.4	36	42	0.05307	0.00501	0.31351	0.02882	0.04284	0.00098	332	166	277	22	270	6	270	102.59
XL131-066	5.3	50	115	0.0546	0.004	0.28589	0.02035	0.03797	0.00071	396	127	255	16	240	4	240	106.25
XL131-067	11	151	235	0.05273	0.00185	0.26472	0.00892	0.03641	0.00039	317	57	238	7	231	2	231	103.03
XL131-068	8.3	110	188	0.05059	0.0028	0.24289	0.01302	0.03482	0.0005	222	97	221	11	221	3	221	100.00
XL131-069	11	163	247	0.05155	0.00184	0.25802	0.00886	0.0363	0.00039	266	59	233	7	230	2	230	101.30
XL131-070	19	253	443	0.05245	0.00196	0.25186	0.00904	0.03482	0.00038	305	62	228	7	221	2	221	103.17

TABLE 3

(continued)

Sample	Pb	Th	U	isotopic ratios						Age (Ma)							
	(ppm)	(ppm)	(ppm)	$^{207}Pb/^{206}Pb$	1σ	$^{207}Pb/^{235}U$	1σ	$^{206}Pb/^{238}U$	1σ	$^{207}Pb/^{206}Pb$	1σ	$^{207}Pb/^{235}U$	1σ	$^{206}Pb/^{238}U$	1σ	Used age	Con%
XL131-071	20	350	460	0.05028	0.00172	0.2277	0.00748	0.03284	0.00034	208	57	208	6	208	2	208	100.00
XL131-072	7.1	101	162	0.05148	0.00282	0.24406	0.01298	0.03438	0.00049	262	96	222	11	218	3	218	101.83
XL131-073	15	90	365	0.05151	0.00142	0.25843	0.00674	0.03638	0.00034	264	43	233	5	230	2	230	101.30
XL131-075	16	210	347	0.05226	0.00208	0.25842	0.0099	0.03586	0.00041	297	66	233	8	227	3	227	102.64
XL131-076	17	219	387	0.05061	0.00205	0.24411	0.00955	0.03498	0.0004	223	69	222	8	222	2	222	100.00
XL131-077	199	68	438	0.15444	0.00183	7.9205	0.07207	0.37196	0.00281	2396	21	2222	8	2039	13	2396	107.83
XL131-080	9.3	129	201	0.04985	0.00222	0.25264	0.01087	0.03675	0.00045	188	77	229	9	233	3	233	98.28
XL131-081	18	103	197	0.05573	0.00145	0.57245	0.01403	0.0745	0.00069	442	38	460	9	463	4	463	99.35
XL131-083	11	167	177	0.05223	0.00245	0.30793	0.01399	0.04276	0.00055	295	80	273	11	270	3	270	101.11
XL131-084	1.8	20	32	0.05197	0.00673	0.3183	0.0403	0.04442	0.00134	284	230	281	31	280	8	280	100.36
XL131-085	12	154	251	0.05008	0.00227	0.25443	0.01116	0.03685	0.00046	199	79	230	9	233	3	233	98.71
XL131-086	8.4	108	189	0.0473	0.00265	0.23372	0.01277	0.03584	0.00049	64	94	213	11	227	3	227	93.83
XL131-087	9.0	115	197	0.05076	0.00185	0.25396	0.00891	0.03628	0.00039	230	61	230	7	230	2	230	100.00
XL131-089	105	60	240	0.11151	0.00141	5.52989	0.05832	0.35966	0.00285	1824	9	1905	9	1981	14	1824	95.75
XL131-090	12	53	213	0.05488	0.00216	0.37307	0.01414	0.0493	0.00053	407	90	322	10	310	3	310	103.87
XL131-091	5.8	72	106	0.04745	0.00416	0.25405	0.02185	0.03883	0.00066	72	194	230	18	246	4	246	93.50
XL131-092	10	126	205	0.05116	0.00174	0.26952	0.0088	0.03821	0.0004	248	56	242	7	242	2	242	100.00
XL131-093	147	207	268	0.15836	0.00183	8.59371	0.07998	0.39359	0.00308	2438	7	2296	8	2139	14	2438	106.18
XL131-094	10	38	207	0.05421	0.00226	0.30694	0.01235	0.04107	0.00046	380	96	272	10	259	3	259	105.02
XL131-096	14	178	279	0.05495	0.00178	0.30164	0.00934	0.03981	0.00041	410	51	268	7	252	3	252	106.35
XL131-097	6.8	69	134	0.05188	0.00268	0.29038	0.01451	0.04059	0.00056	280	89	259	11	256	3	256	101.17
XL131-098	99	119	155	0.15911	0.00187	10.05157	0.09603	0.4582	0.00364	2446	7	2440	9	2432	16	2446	100.25
XL131-100	12	134	241	0.05403	0.00215	0.30093	0.0115	0.04039	0.00047	372	65	267	9	255	3	255	104.71
XL131-101	2.2	13	42	0.05694	0.00503	0.35545	0.03055	0.04528	0.001	489	152	309	23	285	6	285	108.42
XL131-102	10	198	210	0.05121	0.00202	0.25129	0.00956	0.03559	0.0004	250	67	228	8	225	2	225	101.33
XL131-103	5.9	62	134	0.05144	0.00251	0.25587	0.01208	0.03608	0.00047	261	85	231	10	228	3	228	101.32
XL131-104	13	189	259	0.05018	0.00258	0.26917	0.01342	0.0389	0.00053	203	90	242	11	246	3	246	98.37
XL131-105	11	127	238	0.05064	0.00213	0.26858	0.01091	0.03847	0.00045	224	72	242	9	243	3	243	99.59
XL131-106	15	158	320	0.05075	0.00159	0.2635	0.00791	0.03766	0.00037	229	51	237	6	238	2	238	99.58
XL131-107	7.6	86	158	0.05055	0.00259	0.26816	0.0133	0.03847	0.00052	220	90	241	11	243	3	243	99.18
XL131-108	15	186	345	0.05146	0.00163	0.24354	0.00737	0.03432	0.00034	261	51	221	6	218	2	218	101.38
XL131-109	11	141	237	0.05074	0.00197	0.26819	0.01003	0.03834	0.00043	229	66	241	8	243	3	243	99.18
XL131-110	8.8	101	171	0.05573	0.00336	0.30521	0.01793	0.03972	0.00052	442	138	270	14	251	3	251	107.57
XL131-111	9.5	177	185	0.05087	0.00228	0.26114	0.01134	0.03724	0.00046	235	77	236	9	236	3	236	100.00

TABLE 3

(continued)

Sample	Pb (ppm)	Th (ppm)	U (ppm)	isotopic ratios $^{207}Pb/^{206}Pb$	1σ	$^{207}Pb/^{235}U$	1σ	$^{206}Pb/^{238}U$	1σ	Age (Ma) $^{207}Pb/^{206}Pb$	1σ	$^{207}Pb/^{235}U$	1σ	$^{206}Pb/^{238}U$	1σ	Used age	Con%
XL131-071	20	350	460	0.05028	0.00172	0.2277	0.00748	0.03284	0.00034	208	57	208	6	208	2	208	100.00
XL131-112	8.5	100	169	0.05168	0.00201	0.2876	0.01078	0.04037	0.00046	271	65	257	9	255	3	255	100.78
XL131-113	14	180	304	0.05144	0.00201	0.26578	0.00999	0.03748	0.00042	261	66	239	8	237	3	237	100.84
XL131-114	4.9	38	95	0.05075	0.00407	0.27618	0.02172	0.03947	0.00062	230	184	248	17	250	4	250	99.20
XL131-115	6.9	93	136	0.05271	0.0024	0.28349	0.01247	0.03901	0.00049	316	77	253	10	247	3	247	102.43
XL131-118	4.3	42	77	0.05208	0.0044	0.29165	0.02418	0.04061	0.00066	289	193	260	19	257	4	257	101.17
XL131-119	12	144	254	0.0509	0.00161	0.25915	0.00785	0.03693	0.00036	236	52	234	6	234	2	234	100.00
XL131-121	12	193	212	0.05162	0.0018	0.28516	0.00959	0.04007	0.00041	269	58	255	8	253	3	253	100.79
XL131-122	11	139	229	0.05207	0.00262	0.26556	0.01296	0.03699	0.0005	288	87	239	10	234	3	234	102.14
XL131-123	19	276	420	0.05573	0.0024	0.27038	0.01129	0.03519	0.00036	441	98	243	9	223	2	223	108.97
XL131-124	14	162	303	0.05076	0.00221	0.25043	0.01055	0.03579	0.00043	230	75	227	9	227	3	227	100.00
XL131-125	14	205	301	0.05075	0.0016	0.25537	0.00771	0.0365	0.00036	229	51	231	6	231	2	231	100.00

Conc. (%) is percentage concordance defined as $[(^{206}Pb/^{238}U\ age)/(^{207}Pb/^{206}Pb\ age)] \times 100$.

TABLE 4

Lu-Hf isotopic data of detrital zircons from sandstones in the Xinglonggou Formation, western Liaoning

Sample	used age (Ma)	$^{176}Yb/^{177}Hf$	$^{176}Lu/^{177}Hf$	$^{176}Hf/^{177}Hf$	2σ	$\varepsilon_{Hf}(0)$	$\varepsilon_{Hf}(t)$	2σ	T_{DM2}(Ma)	$f_{Lu/Hf}$
XL130-02	2477	0.009097	0.000400	0.281327	0.000026	-51.1	3.8	1.4	2694	-0.99
XL130-04	287	0.012384	0.000511	0.282769	0.000032	-0.1	6.1	1.5	793	-0.98
XL130-07	243	0.011449	0.000539	0.282725	0.000024	-1.7	3.6	1.3	887	-0.98
XL130-08	2327	0.005936	0.000229	0.281378	0.000032	-49.3	2.5	1.6	2637	-0.99
XL130-10	327	0.012478	0.000601	0.282438	0.000026	-11.8	-4.7	1.4	1379	-0.98
XL130-11	2384	0.006656	0.000271	0.281331	0.000034	-50.9	2.1	1.6	2705	-0.99
XL130-15	231	0.025427	0.001061	0.282777	0.000026	0.2	5.1	1.4	800	-0.97
XL130-20	255	0.013371	0.000610	0.282493	0.000034	-9.8	-4.4	1.6	1301	-0.98
XL130-21	253	0.018805	0.000787	0.282782	0.000038	0.3	5.8	1.7	782	-0.98
XL130-22	222	0.022339	0.000912	0.282797	0.000030	0.9	5.6	1.5	765	-0.97
XL130-23	220	0.017480	0.000769	0.282753	0.000038	-0.7	4.0	1.7	845	-0.98
XL130-33	250	0.012457	0.000632	0.282398	0.000028	-13.2	-7.8	1.4	1474	-0.98
XL130-35	221	0.021875	0.000937	0.282905	0.000040	4.7	9.4	1.7	569	-0.97
XL130-36	218	0.019919	0.000871	0.282823	0.000032	1.8	6.5	1.5	719	-0.97
XL130-38	238	0.020224	0.000884	0.282801	0.000042	1.0	6.1	1.8	753	-0.97
XL130-40	2441	0.013058	0.000527	0.281463	0.000046	-46.3	7.6	2.0	2477	-0.98
XL130-41	2480	0.008072	0.000338	0.281284	0.000044	-52.6	2.5	1.9	2764	-0.99
XL130-47	233	0.022003	0.000917	0.282788	0.000028	0.5	5.5	1.4	778	-0.97
XL130-48	250	0.025887	0.000974	0.282802	0.000046	1.0	6.4	1.9	749	-0.97
XL130-52	234	0.024157	0.001001	0.282825	0.000032	1.9	6.8	1.5	711	-0.97
XL130-53	231	0.021110	0.000892	0.282838	0.000032	2.3	7.3	1.5	688	-0.97
XL130-54	231	0.021382	0.000900	0.282846	0.000032	2.6	7.5	1.5	673	-0.97
XL130-58	2486	0.013344	0.000548	0.281338	0.000044	-50.7	4.2	1.9	2685	-0.98
XL130-63	2416	0.013309	0.000541	0.281265	0.000040	-53.3	0.0	1.8	2833	-0.98
XL130-66	2379	0.009487	0.000403	0.281376	0.000034	-49.4	3.3	1.6	2639	-0.99
XL130-68	215	0.026685	0.001154	0.282793	0.000028	0.7	5.3	1.4	776	-0.97
XL130-74	1614	0.011408	0.000458	0.281282	0.000026	-52.7	-17.3	1.7	3039	-0.99
XL130-78	234	0.022657	0.000958	0.282795	0.000040	0.8	5.8	1.7	766	-0.97
XL130-79	285	0.016619	0.000751	0.282513	0.000046	-9.1	-3.0	1.9	1258	-0.98
XL130-81	246	0.027105	0.001094	0.282776	0.000030	0.1	5.4	1.5	798	-0.97
XL130-82	224	0.022985	0.000937	0.282830	0.000017	2.0	6.8	1.2	705	-0.97
XL130-84	242	0.020918	0.000873	0.282812	0.000034	1.4	6.6	1.6	732	-0.97
XL130-86	264	0.018796	0.000859	0.282410	0.000026	-12.8	-7.1	1.4	1450	-0.97
XL130-87	245	0.020075	0.000866	0.282830	0.000032	2.0	7.3	1.5	698	-0.97

Table 4

(continued)

Sample	used age (Ma)	$^{176}Yb/^{177}Hf$	$^{176}Lu/^{177}Hf$	$^{176}Hf/^{177}Hf$	2σ	$\varepsilon_{Hf}(0)$	$\varepsilon_{Hf}(t)$	2σ	T_{DM2}(Ma)	$f_{Lu/Hf}$
XL130-89	2452	0.009188	0.000397	0.281304	0.000028	-51.9	2.5	1.5	2742	-0.99
XL130-92	222	0.023736	0.001005	0.282805	0.000032	1.2	5.9	1.5	751	-0.97
XL130-95	224	0.022568	0.000950	0.282732	0.000028	-1.4	3.3	1.4	883	-0.97
XL130-96	227	0.018448	0.000782	0.282831	0.000026	2.1	6.9	1.4	701	-0.98
XL130-97	237	0.020800	0.000816	0.282623	0.000050	-5.3	-0.2	2.0	1075	-0.98
XL130-99	2499	0.007930	0.000313	0.281327	0.000034	-51.1	4.5	1.6	2680	-0.99
XL130-100	2584	0.015543	0.000611	0.281292	0.000022	-52.3	4.7	1.3	2741	-0.98
XL130-105	250	0.020477	0.000880	0.282856	0.000028	3.0	8.3	1.4	650	-0.97
XL130-106	244	0.017866	0.000739	0.282637	0.000036	-4.8	0.5	1.6	1047	-0.98
XL130-112	249	0.015970	0.000683	0.282802	0.000044	1.0	6.4	1.9	746	-0.98
XL130-113	222	0.023272	0.000901	0.282697	0.000038	-2.7	2.1	1.7	947	-0.97
XL130-115	233	0.021200	0.000883	0.282805	0.000048	1.2	6.1	2.0	747	-0.97
XL130-119	220	0.027606	0.001151	0.282922	0.000042	5.3	10.0	1.8	540	-0.97
XL131-001	247	0.000905	0.282770	0.026175	0.001880	-0.1	5.2	2.0	806	-0.97
XL131-002	227	0.000993	0.282823	0.030098	0.002600	1.8	6.6	1.9	716	-0.97
XL131-003	223	0.000732	0.282546	0.021855	0.001040	-8.0	-3.2	1.6	1217	-0.98
XL131-004	216	0.002646	0.282923	0.078011	0.005800	5.3	9.7	1.8	549	-0.92
XL131-005	2442	0.000491	0.281338	0.016803	0.001920	-50.7	3.3	1.9	2694	-0.99
XL131-006	259	0.001687	0.282451	0.057173	0.008000	-11.4	-6.0	2.0	1386	-0.95
XL131-009	233	0.001634	0.282812	0.049782	0.000540	1.4	6.3	2.0	739	-0.95
XL131-010	214	0.001119	0.282909	0.034596	0.001560	4.8	9.4	1.7	564	-0.97
XL131-011	239	0.001024	0.282947	0.030070	0.001540	6.2	11.3	2.0	487	-0.97
XL131-012	221	0.001154	0.282848	0.035172	0.003600	2.7	7.4	1.7	674	-0.97
XL131-013	230	0.001063	0.282730	0.033397	0.001300	-1.5	3.4	2.0	885	-0.97
XL131-014	229	0.001170	0.282781	0.036153	0.000620	0.3	5.2	2.0	793	-0.96
XL131-015	236	0.000873	0.282707	0.025625	0.001400	-2.3	2.8	2.1	923	-0.97
XL131-017	228	0.001229	0.282762	0.037665	0.004800	-0.4	4.5	2.0	828	-0.96
XL131-020	224	0.001219	0.282866	0.038001	0.006000	3.3	8.1	1.8	640	-0.96
XL131-021	244	0.001116	0.282710	0.033566	0.003200	-2.2	3.0	1.6	917	-0.97
XL131-022	237	0.001124	0.282792	0.034789	0.002000	0.7	5.7	2.0	771	-0.97
XL131-023	232	0.001140	0.282846	0.032919	0.000940	2.6	7.5	1.7	674	-0.97
XL131-024	237	0.000751	0.282762	0.022024	0.001800	-0.4	4.7	1.7	822	-0.98
XL131-026	234	0.001144	0.282828	0.032628	0.001820	2.0	6.9	1.9	706	-0.97
XL131-028	244	0.000833	0.282918	0.024730	0.004200	5.2	10.4	1.6	537	-0.97
XL131-029	222	0.001517	0.282818	0.046770	0.004200	1.6	6.3	1.9	731	-0.95

TABLE 4
(continued)

Sample	used age (Ma)	$^{176}Yb/^{177}Hf$	$^{176}Lu/^{177}Hf$	$^{176}Hf/^{177}Hf$	2σ	$\varepsilon_{Hf}(0)$	$\varepsilon_{Hf}(t)$	2σ	T_{DM2}(Ma)	$f_{Lu/Hf}$
XL131-030	245	0.000589	0.282581	0.018357	0.001800	-6.8	-1.5	2.0	1146	-0.98
XL131-031	224	0.001132	0.282889	0.033602	0.001900	4.1	8.9	1.9	598	-0.97
XL131-032	208	0.001309	0.282952	0.038490	0.000600	6.4	10.8	1.5	489	-0.96
XL131-033	243	0.000513	0.282406	0.012977	0.000660	-12.9	-7.7	1.6	1462	-0.98
XL131-034	229	0.001236	0.282911	0.037402	0.001100	4.9	9.8	1.9	557	-0.96
XL131-035	245	0.000626	0.282831	0.017099	0.003200	2.1	7.4	1.8	693	-0.98
XL131-036	228	0.001440	0.282863	0.041572	0.001060	3.2	8.0	1.6	647	-0.96
XL131-037	262	0.000492	0.282449	0.014107	0.001060	-11.4	-5.8	1.9	1378	-0.99
XL131-038	227	0.000954	0.282837	0.027524	0.002200	2.3	7.1	2.0	690	-0.97
XL131-039	212	0.000912	0.282903	0.025631	0.000480	4.6	9.2	1.4	574	-0.97
XL131-041	249	0.001011	0.282858	0.029093	0.001520	3.0	8.4	1.7	646	-0.97
XL131-042	221	0.000906	0.282846	0.026365	0.003000	2.6	7.3	2.0	675	-0.97
XL131-044	234	0.000991	0.282859	0.028912	0.000420	3.1	8.1	2.0	649	-0.97
XL131-045	1784	0.000890	0.281600	0.028806	0.001260	-41.4	-2.8	1.8	2456	-0.97
XL131-047	230	0.001096	0.282885	0.033422	0.002600	4.0	8.9	2.0	603	-0.97
XL131-048	239	0.001098	0.282920	0.031803	0.001300	5.2	10.3	1.9	537	-0.97
XL131-049	232	0.001243	0.282885	0.037518	0.002400	4.0	8.9	1.4	604	-0.96
XL131-052	246	0.002135	0.282918	0.066864	0.008400	5.2	10.2	1.9	547	-0.94
XL131-053	233	0.001087	0.282747	0.030819	0.000600	-0.9	4.1	1.8	853	-0.97
XL131-054	227	0.001130	0.282821	0.035829	0.007000	1.7	6.6	1.9	721	-0.97
XL131-055	234	0.001093	0.282899	0.032640	0.001300	4.5	9.5	1.6	577	-0.97
XL131-056	256	0.001130	0.282415	0.034515	0.002400	-12.6	-7.2	1.6	1447	-0.97
XL131-057	232	0.001097	0.282880	0.032428	0.001600	3.8	8.8	1.7	612	-0.97
XL131-058	234	0.000951	0.282753	0.027299	0.001220	-0.7	4.3	2.0	841	-0.97
XL131-059	226	0.000774	0.282835	0.023176	0.002600	2.2	7.1	1.8	693	-0.98
XL131-060	240	0.000906	0.282996	0.026377	0.000920	7.9	13.1	1.8	396	-0.97
XL131-061	234	0.000648	0.282893	0.018494	0.000880	4.3	9.3	1.5	584	-0.98
XL131-062	251	0.001945	0.282597	0.058985	0.006600	-6.2	-1.0	1.8	1127	-0.94
XL131-063	2426	0.000451	0.281251	0.014000	0.000500	-53.8	-0.1	1.9	2848	-0.99
XL131-064	236	0.001252	0.282756	0.037422	0.001360	-0.6	4.4	1.7	837	-0.96
XL131-065	270	0.000584	0.282196	0.017887	0.001400	-20.4	-14.5	2.0	1831	-0.98
XL131-066	240	0.000641	0.282968	0.017183	0.000260	6.9	12.1	1.9	445	-0.98
XL131-067	231	0.001230	0.282980	0.035208	0.002800	7.4	12.3	1.7	431	-0.96
XL131-068	221	0.001048	0.282820	0.028986	0.001220	1.7	6.4	1.8	724	-0.97
XL131-069	230	0.001145	0.282941	0.032519	0.004600	6.0	10.9	1.9	502	-0.97

TABLE 4

(continued)

Sample	used age (Ma)	$^{176}Yb/^{177}Hf$	$^{176}Lu/^{177}Hf$	$^{176}Hf/^{177}Hf$	2σ	$\varepsilon_{Hf}(0)$	$\varepsilon_{Hf}(t)$	2σ	T_{DM2}(Ma)	$f_{Lu/Hf}$
XL131-070	221	0.001322	0.282827	0.038485	0.002600	1.9	6.6	2.0	713	-0.96
XL131-071	208	0.001416	0.282938	0.040969	0.008800	5.9	10.3	1.7	515	-0.96
XL131-072	218	0.000915	0.282867	0.025052	0.000980	3.4	8.0	1.8	638	-0.97
XL131-073	230	0.000941	0.282686	0.022894	0.000420	-3.0	1.9	2.0	963	-0.97
XL131-075	227	0.001059	0.283012	0.030322	0.001100	8.5	13.3	1.5	372	-0.97
XL131-076	222	0.001114	0.282778	0.032782	0.002200	0.2	4.9	1.9	800	-0.97
XL131-077	2396	0.000210	0.281388	0.006035	0.000420	-48.9	4.5	1.6	2598	-0.99
XL131-080	233	0.001244	0.282788	0.034453	0.002800	0.6	5.5	2.0	780	-0.96
XL131-081	463	0.000897	0.282658	0.022778	0.000860	-4.0	5.9	1.8	947	-0.97
XL131-083	270	0.000673	0.282365	0.022734	0.000820	-14.4	-8.6	1.3	1529	-0.98
XL131-084	280	0.000392	0.282165	0.012109	0.000380	-21.5	-15.4	1.8	1882	-0.99
XL131-085	233	0.001304	0.282911	0.037905	0.001980	4.9	9.8	2.0	557	-0.96
XL131-086	227	0.001358	0.282748	0.038924	0.001360	-0.8	3.9	1.6	855	-0.96
XL131-089	1824	0.000267	0.281610	0.007408	0.000300	-41.1	-0.8	2.0	2389	-0.99
XL131-090	310	0.001068	0.282890	0.030848	0.000520	4.2	10.8	1.4	571	-0.97
XL131-091	246	0.001374	0.282862	0.041304	0.004400	3.2	8.4	1.7	643	-0.96
XL131-092	242	0.001138	0.282878	0.033368	0.001600	3.8	8.9	1.7	613	-0.97
XL131-093	2438	0.000774	0.281353	0.022648	0.001800	-50.2	3.2	1.5	2692	-0.98
XL131-094	259	0.000712	0.282679	0.017663	0.001720	-3.3	2.3	1.7	966	-0.98
XL131-096	252	0.001204	0.282837	0.035160	0.001620	2.3	7.6	1.8	685	-0.96
XL131-097	256	0.000908	0.282882	0.026151	0.000780	3.9	9.4	1.9	600	-0.97
XL131-098	2446	0.000788	0.281272	0.025379	0.002400	-53.0	0.5	1.7	2832	-0.98
XL131-100	255	0.000666	0.282456	0.017180	0.001740	-11.2	-5.7	1.6	1369	-0.98
XL131-101	285	0.001010	0.282915	0.026638	0.001200	5.1	11.1	1.8	532	-0.97
XL131-102	225	0.001161	0.282897	0.032690	0.002600	4.4	9.2	2.0	583	-0.97
XL131-103	228	0.001138	0.282851	0.031228	0.002400	2.8	7.6	1.8	666	-0.97
XL131-104	246	0.000813	0.282522	0.022165	0.000400	-8.8	-3.6	1.7	1254	-0.98
XL131-105	243	0.000870	0.282729	0.025316	0.001600	-1.5	3.7	2.0	881	-0.97
XL131-106	238	0.001079	0.282664	0.032289	0.002800	-3.8	1.2	1.7	1002	-0.97
XL131-107	243	0.000912	0.282857	0.026715	0.002400	3.0	8.2	1.8	649	-0.97
XL131-108	218	0.001117	0.282880	0.033150	0.000960	3.8	8.5	2.0	616	-0.97
XL131-109	243	0.001131	0.282922	0.033473	0.002000	5.3	10.5	1.8	532	-0.97
XL131-110	251	0.001060	0.282912	0.030264	0.001960	5.0	10.3	1.9	548	-0.97
XL131-111	236	0.001379	0.282737	0.041197	0.007600	-1.2	3.7	1.9	873	-0.96
XL131-112	255	0.001239	0.282722	0.036954	0.001960	-1.8	3.6	2.0	894	-0.96

TABLE 4

(continued)

Sample	used age (Ma)	$^{176}Yb/^{177}Hf$	$^{176}Lu/^{177}Hf$	$^{176}Hf/^{177}Hf$	2σ	$\varepsilon_{Hf}(0)$	$\varepsilon_{Hf}(t)$	2σ	T_{DM2}(Ma)	$f_{Lu/Hf}$
XL131-113	237	0.001329	0.282851	0.041211	0.003800	2.8	7.8	2.0	665	-0.96
XL131-114	250	0.000116	0.282646	0.003882	0.000178	-4.5	1.0	1.9	1023	-1.00
XL131-115	247	0.000844	0.282914	0.024562	0.001460	5.0	10.3	1.9	544	-0.97
XL131-118	257	0.000596	0.282863	0.017467	0.000940	3.2	8.8	1.9	631	-0.98
XL131-119	234	0.001042	0.282899	0.030725	0.001260	4.5	9.5	1.9	576	-0.97
XL131-121	253	0.001863	0.282827	0.058148	0.001920	1.9	7.2	1.9	709	-0.94
XL131-122	234	0.001140	0.282758	0.034087	0.001520	-0.5	4.5	1.7	833	-0.97
XL131-123	223	0.001012	0.282856	0.030271	0.000660	3.0	7.7	1.4	657	-0.97
XL131-124	227	0.001087	0.282765	0.031675	0.002200	-0.2	4.6	2.0	822	-0.97
XL131-125	231	0.001003	0.282834	0.030454	0.000580	2.2	7.1	1.9	695	-0.97

The initial $^{176}Hf/^{177}Hf$ ratios were calculated with reference to the chondritic reservoir (CHUR) at the time of zircon growth from magmas. $\varepsilon_{Hf}(t)$ values are defined to denote a 0.1 per mil difference between the sample and the chondritic reservoir at the time of magma crystallization. The decay constant for ^{176}Lu and the chondritic ratios of $^{176}Hf/^{177}Hf$ and $^{176}Lu/^{177}Hf$ used in calculations are 1.867×10^{-11} yr^{-1} (Scherer and others, 2001) and 0.282772 and 0.0332 (Bichert-Toft and Albarède, 1997), respectively. A two-stage continental model age (T_{DM2}) was calculated by projecting the initial $^{176}Hf/^{177}Hf$ of zircon back to the depleted mantle growth curve using $^{176}Lu/^{177}Hf = 0.0093$ for the upper continental crust (Vervoort and Patchett, 1996).

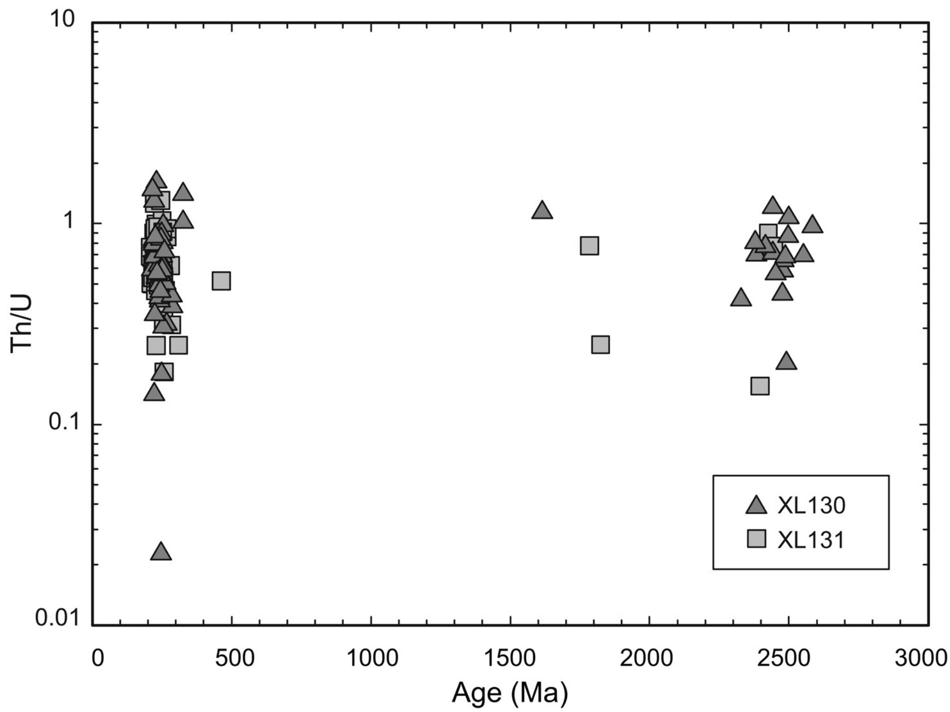

Fig. 5. Plots of Th/U ratios versus U-Pb ages of concordant detrital zircons.

125 zircon grains were analyzed and 103 concordant ages were obtained on XL131. The concordant zircons show similar two major age populations: 260 to 220 Ma and ca. 2400 Ma (figs. 6 and 7). Only two grains give the age of ~1.8 Ga. Two grains yield the identical youngest age 208 Ma (Spot XL130-032 and XL130-071) and the oldest age is 2446±67 Ma (Spot XL130-098).

Hf Isotopes

149 representative concordant grains out of the dated 246 zircons were analyzed for the Hf isotopes (table 4). As shown in figure 8, the ε_{Hf} (t) values exhibit distinctive characteristics for different U-Pb age groups. Majority of the 2.6 to 2.4 Ga zircons have positive ε_{Hf} (t) up to the depleted mantle (DM) value and crustal model ages of 2.8 to 2.5 Ga. The 3 grains with U-Pb age of 1.9 to 1.6 Ga have ε_{Hf} (t) values of −0.8 to −17.3 and crustal model ages of 3.0 to 2.4 Ga. However, ε_{Hf} (t) values of the 260 to 220 Ma zircons range widely from −15.4 to 13.3 and 127 zircons of them have positive ε_{Hf} (t) values although 22 grains have the negative values. Again, the high values almost reach the depleted mantle value (fig. 8) and suggest juvenile crustal additions. The 260 to 220 Ma zircons have crustal model ages of 1882 to 372 Ma.

DISCUSSION

Source of Sandstones

As shown in figure 5, majority of the zircons have Th/U>0.50 characteristic of an igneous origin (Hanchar and Hoskin, 2003). Typical metamorphic Th/U ratios (<0.10) occur only for one zircon (XL130-57). Except for XL130-57 (Th/U=0.02), all

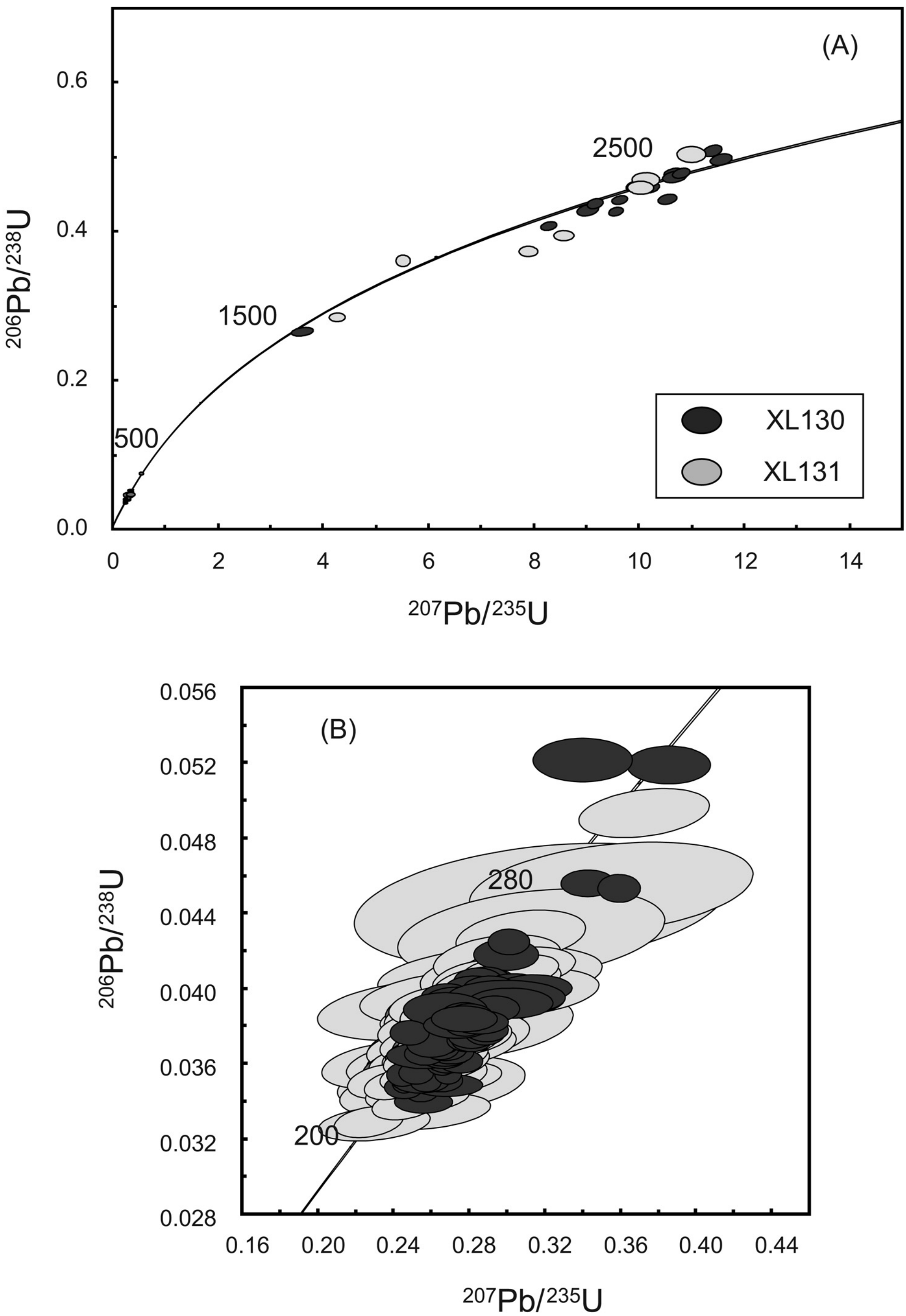

Fig. 6. U-Pb concordia ages of all detrital zircons (A) and Phanerozoic detrital zircons only (B) from the Xinglonggou Formation.

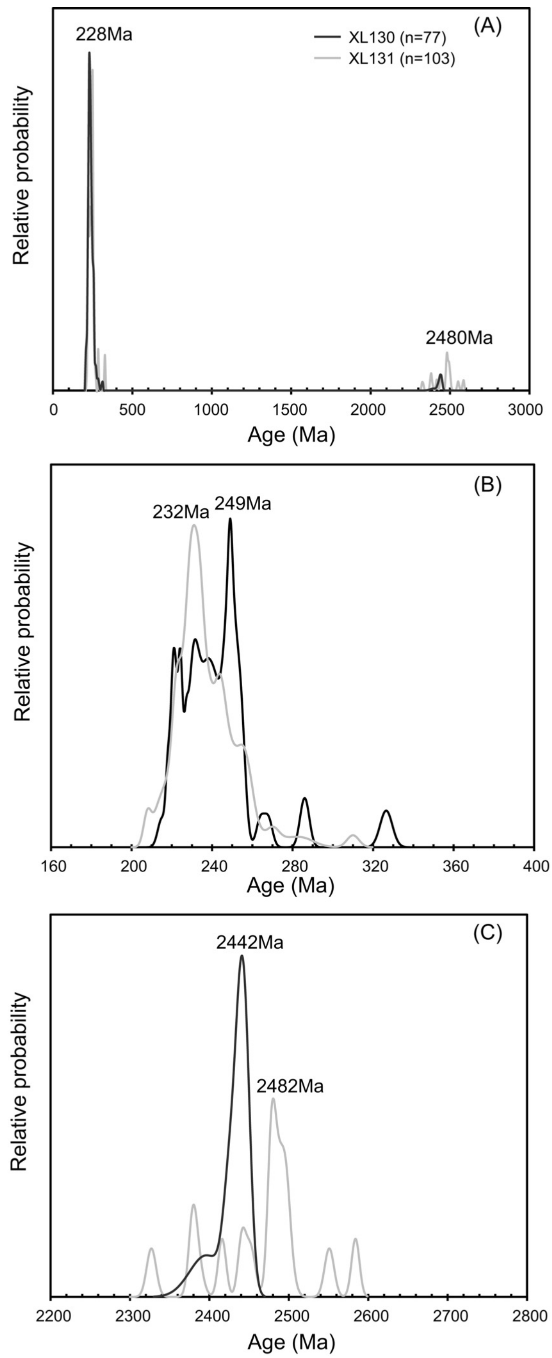

Fig. 7. Relative probability plots of U-Pb ages for all concordant detrital zircons (A), Phanerozoic concordant detrital zircons (B), and Precambrian concordant detrital zircons (C) from the Xinglonggou Formation.

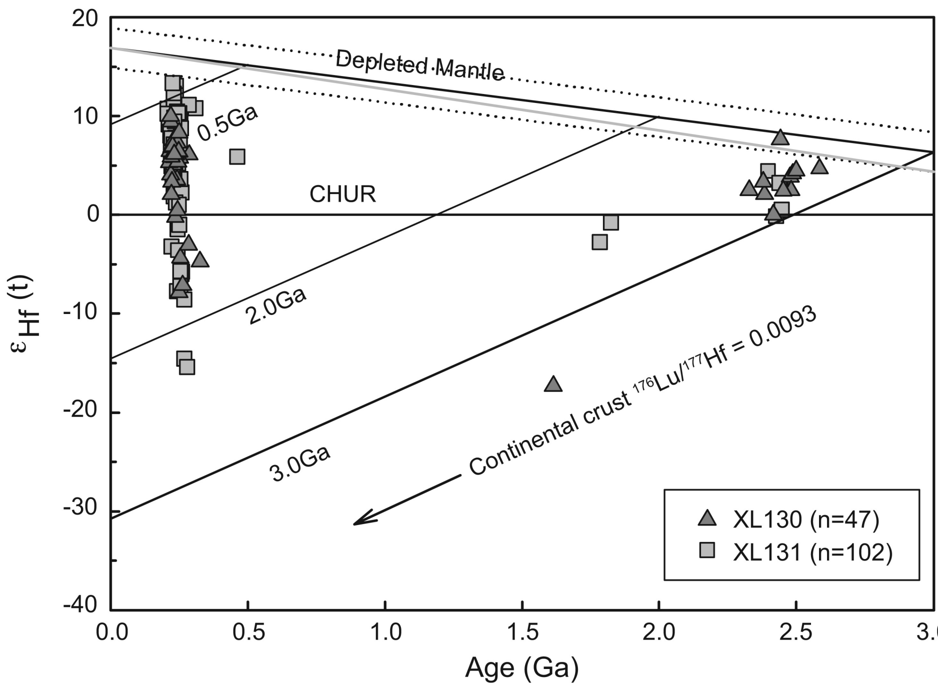

Fig. 8. U-Pb ages versus ε_{Hf} (t) value plots of concordant detrital zircons from the Xinglonggou Formation. The depleted mantle growth curve (black solid line) was calculated assuming a present-day $^{176}Hf/^{177}Hf = 0.28325$, $^{176}Lu/^{177}Hf = 0.0384$ (Griffin and others, 2002) and the dotted lines represent two ε_{Hf} units variation of the depleted mantle growth curve. The gray line represents depleted mantle growth curve based on zircon data (Pietranik and others, 2009).

the zircons show similar characteristics of "magmatic-like" zircon REE patterns with high positive Ce anomalies and steep increase from La to Lu (Pelleter and others, 2007). The results are consistent with the CL images predominated by oscillatory zoning typical of igneous origin (fig. 3).

As shown in figures 6 and 7, although the obtained zircon ages show a wide range from 2584 to 208 Ma, major age groups peak at 228 Ma and 2480 Ma (fig. 7A). They account for 87.2 percent and 11.2 percent of the total population, respectively. In addition, three grains range from 1.9 to 1.6 Ga. Only three grains give the age of 330 to 300 Ma. In detail, the 260 to 220 Ma zircons show a major peak at 232 Ma and 249 Ma (fig. 7B). The youngest U-Pb age (208 Ma), which can be used to define the maximum depositional age of sedimentary rocks (Nelson, 2001; Yang and others, 2006; Li and others, 2007; Kirkland and others, 2008; Liu and others, 2008), indicates a maximum depositional age of Late Triassic time for the Xinglonggou Formation.

Zircon ages of the Precambrian basements of the North China craton mainly range from 2.8 to 2.5 Ga with a peak at 2.5 Ga (Zhao and others, 2001; Gao and others, 2004). As described above, some of the 2.5 Ga zircons show positive ε_{Hf} (t) value high up to coeval depleted mantle values with Hf model age of 2.8 to 2.5 Ga, indicative of juvenile crustal additions. Similar Hf isotopic compositions of the ca. 2.5 Ga zircons investigated in this study with that from the North China Archean basements indicates a common source (Yang and others, 2005; Yang and others, 2009). In addition to the ca. 2.5 Ga zircons, 1.9 to 1.6 Ga zircons are also abundant in the North China craton (Zhao and others, 2001). The 1.9 to 1.6 Ga zircons have negative ε_{Hf} (t) values and

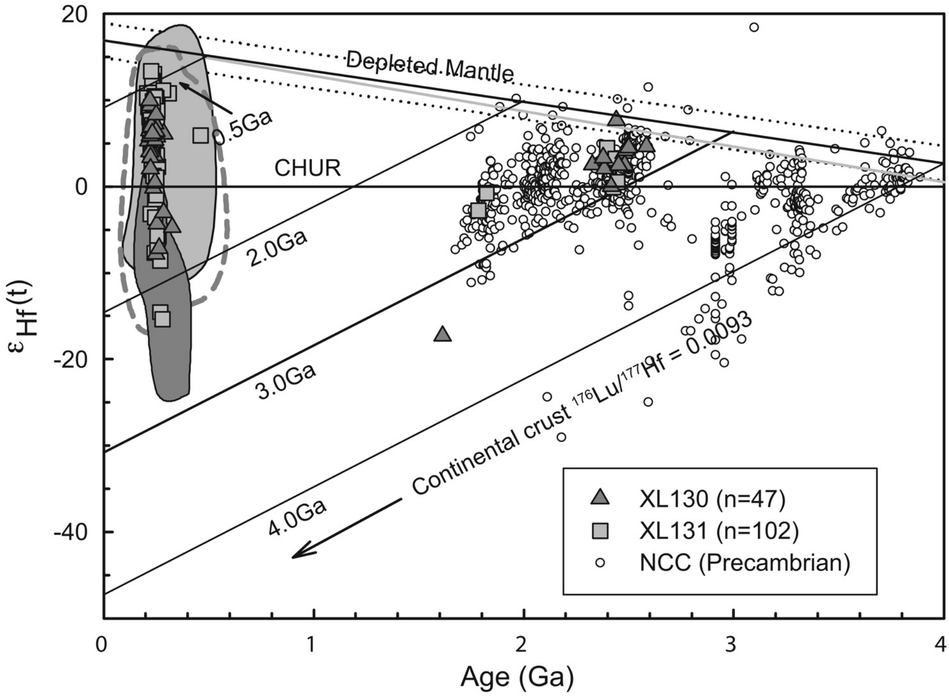

Fig. 9. Compilation of ε_{Hf} (t) vs. U-Pb ages of zircons from the North China craton and the eastern Central Asian Orogenic Belt. Depleted mantle growth lines are the same as in figure 8. The solid symbols represent the data from this study. Dashed line area represents detrital zircons from modern rivers covering the entire northeastern China, which comprises much of eastern Central Asian Orogenic Belt (Li, ms, 2010). Gray and dark gray areas indicate the Phanerozoic zircons from the eastern Central Asian Orogenic Belt (Zhou and others, 2005; Cheng and others, 2006; Chen and others, 2009) and the North China craton (Zheng and others, 2004; Wu and others, 2005b, 2008; Yang and others, 2006, 2007; Li and others, 2007; Tian and others, 2007; Wan and others, 2007; Zhang and others, 2007b; Luo and others, 2008), respectively.

their T_{DM2} ages vary from 3.0 to 2.4 Ga. These suggest remarkable reworking of pre-existing Archean crustal materials at 1.9 to 1.6 Ga. In contrast, rare Precambrian zircons were found in rocks of the eastern Central Asian Orogenic Belt (Yang and others, 2006; Chen and others, 2009). Previously identified Proterozoic metamorphic rocks are now considered to be Paleozoic in age (for example, Miao and others, 2004). The Jiamusi Massif is a Precambrian micro-continental block whose metamorphic age has been precisely dated at 500 Ma by SHRIMP zircon analyses (Wilde and others, 1997; 2000). These observations well document that the Precambrian zircons in the Xinglonggou sandstones were derived from the North China craton.

Phanerozoic igneous rocks are also present in the North China craton. Intrusive rocks, including diorite, granodiorite, monzogranite, syenogranite, A-type granite and syenite, and associated volcanic rocks, have zircon U-Pb ages of 390 to 111 Ma (for example, Luo and others, 2001, 2003; Miao and others, 2002, 2003; Gao and others, 2004; Han and others, 2004; Ma and others, 2004; Zhang and others, 2004, 2007a; 2007b, 2009a, 2009b; Wu and others, 2005a, 2005c, 2006; Yang and others, 2007, 2008). The whole-rock Nd isotopic data for the volcanic rocks of the North China craton show negative ε_{Nd} (t) values and older Nd model ages. Hf isotopes also give the same conclusion, Phanerozoic zircons from the North China craton have negative ε_{Hf} (t) values (fig. 9) and ancient Hf model ages (fig. 10) (Yang and others, 2006, 2007; Wu and others, 2007; Zhang and others, 2007b). According to the existing data, the

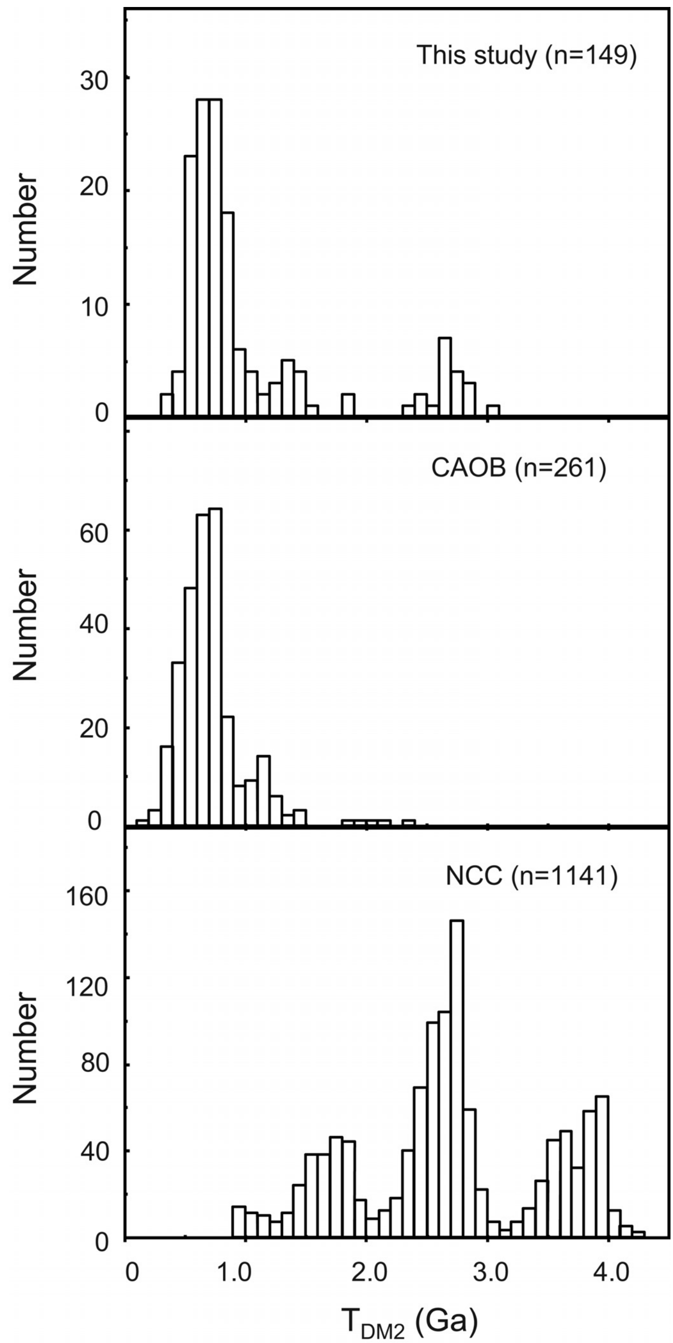

Fig. 10. Histogram of T_{DM2} ages of zircons from Xinglonggou Formation compared to igneous zircons from the North China craton (NCC) (Zheng and others, 2004; Wu and others, 2005b, 2008; Yang and others, 2006, 2007; Li and others, 2007; Tian and others, 2007; Wan and others, 2007; Zhang and others, 2007b; Luo and others, 2008) and the eastern Central Asian Orogenic Belt (CAOB) (Zhou and others, 2005; Cheng and others, 2006; Chen and others, 2009).

positive values in the North China craton were reported only by Yang and others (2006) for detrital zircons from western Beijing and Tian and others (2007) from northern Hebei, which have been interpreted as being derived from the Central Asian Orogenic Belt source or affected by subduction of the Paleo-Asian ocean.

In contrast, Phanerozoic zircons are distinct in the eastern Central Asian Orogenic Belt. The eastern segment of the Central Asian Orogenic Belt includes eastern and southern central Mongolia, northern Inner Mongolia of China, and northeastern China. The granites are dominant with rare mafic rocks. The ages of these rocks range from Late Paleozoic to Late Mesozoic (280-120 Ma) (Chen and others, 2000, 2009; Sun and others, 2000; Wu and others, 2000, 2002, 2003a; Jahn and others, 2001; Fan and others, 2003; Wang and others, 2004; Shi and others, 2004; Ge and others, 2005; Liu and others, 2005; Cheng and others, 2006; Jian and others, 2008; Miao and others, 2008; Zhang and others, 2008; Xu and others, 2009). Several plutons have been identified as early Paleozoic in age using the whole rock Rb-Sr method, which are considered to be unreliable. The granites of early Paleozoic age are not as widespread as previously thought. The well dated early Paleozoic plutons are distributed mainly along the northern margin of northeastern China (Ge and others, 2005; Zhou and others, 2005) and northern Inner Mongolia (Chen and others, 2000, 2009). Granitoids with ages mainly from 270 to 120 Ma are characterized by low initial Sr isotopic ratios and generally positive ε_{Nd} (t) values and young Nd model ages (for example, Shao and others, 1999; Chen and others, 2000, 2009; Jahn and others, 2000a, 2000b, 2004; Wu and others, 2000, 2002, 2003b, 2007; Miao and others, 2008; Zhang and others, 2008; Xu and others, 2009). Granitoids with negative ε_{Nd} (t) values also exist, but they occur in Precambrian blocks (for example, the Jiamusi Massif) and their isotopic compositions reflect contamination of the older crust in the magma generation. This characteristic also existed in other parts of the Central Asian Orogenic Belt (for example, Jahn, 2004; Kovalenko and others, 2004; Sun and others, 2008; Wang and others, 2009). Coupled with the whole-rock Nd isotopes, the Phanerozoic zircons from the eastern Central Asian Orogenic Belt have positive ε_{Hf} (t) values (fig. 9) and younger Hf model ages (fig. 10) (Zhou and others, 2005; Cheng and others, 2006; Yang and others, 2006; Chen and others, 2009). In summary, Phanerozoic zircons from the North China craton and the eastern Central Asian Orogenic Belt are distinct.

In this study, the Phanerozoic zircons mostly have the ages between 260 to 220 Ma, with only three zircons having ages of 330 to 300 Ma. As we discussed above, both the shape of the zircons and presence of amphibole in the sandstones support a near source for the Xinglonggou sandstones. This is reinforced by the restricted age populations of the zircon. The early Paleozoic ages in the eastern Central Asian Orogenic Belt were mainly distributed along the northern margin of northeastern China (Ge and others, 2005; Zhou and others, 2005) and northern Inner Mongolia (Chen and others, 2000, 2009), which lie in the northern Solonker suture and may have no or rare contribution to the Xinglonggou sandstones. A Late Carboniferous-Early Permian (ca. 330-298 Ma) Andean-style continental arc existed along the northern margin of the North China craton (Zhang and others, 2007a, 2009a). The 330 to 300 Ma zircons might have been derived from the Carboniferous magmatic arc along the northern margin of the North China craton with zircon U-Pb ages of 324 to 310 Ma (Zhang and others, 2004). However, the 260 to 220 Ma Xinglonggou zircons are characterized by positive ε_{Hf} (t) values and young Hf model ages, which are distinct from the North China craton zircons but similar to the eastern Central Asian Orogenic Belt zircons (figs. 9 and 10). Thus, the Xinglonggou zircons are mixtures of sources from the North China craton and eastern Central Asian Orogenic Belt with the predominance of the latter.

Triassic Crustal Growth and Tectonic Evolution

The Central Asian Orogenic Belt, which is the largest Phanerozoic accretionary orogen in the world (Sengör and others, 1993; Sengör and Natal'in, 1996), is critical to the study of continental crustal growth and geological history of central Asia. Phanerozoic crustal growth is evidenced by the emplacement of voluminous granitoids with low initial $^{87}Sr/^{86}Sr$, generally positive ε_{Nd} (t) values and young Nd model ages (Shao and others, 1999; Chen and others, 2000; Jahn and others, 2000, 2004; Wu and others, 2002, 2007). Such juvenile isotopic signatures are also exhibited by Phanerozoic granitoids in areas like New England, the Cordillera of North America (Samson and others, 1989; Pickett and Saleeby, 1999), Newfoundland Appalachians in Canada (Whalen and others, 1996) and Africa (Kinnaird and Bowden, 1987).

These studies are based on whole-rock analysis which may be compromised by mixing processes. *In-situ* analysis of Lu-Hf isotopic compositions of zircons provides less ambiguous timing of the crustal growth. Meanwhile, the Lu-Hf isotopic system of zircons is relatively immune to tectono-thermal events. As discussed above, 260 to 220 Ma Xinglonggou zircons show a wide range of ε_{Hf} (t) values from close to depleted mantle values to slightly negative values. These zircons can be interpreted by mixing of Permian-Triassic (260-220 Ma) new crustal additions with recycled Precambrian crust. The continuous ε_{Hf} (t) variation and the large number of zircons with positive ε_{Hf} (t) values suggest a possible magma mixing process with juvenile magma as the major component.

Two lines of evidence suggest that the Permian-Triassic (260-220 Ma) crustal growth documented by the Xinglonggou detrital zircons was widespread and significant for the entire eastern Central Asian Orogenic Belt. On one hand, 105 out of 167 concordant detrital zircons from modern rivers well covering the entire northeastern China, which comprises much of eastern Central Asian Orogenic Belt, also show positive ε_{Hf} up to the depleted mantle value for one of the major age groups at 270 to 210 Ma (see fig. 1A and fig. 9) (Li, ms, 2010). On the other hand, Permian-Triassic granitoids whose zircons show positive ε_{Hf} at the time of magma crystallization up to the depleted mantle value are voluminous in the eastern Central Asian Orogenic Belt (Cheng and others, 2006; Yang and others, 2006; Chen and others, 2009) (fig. 9).

As described above, previous studies of ophiolites and post-collision intrusive rocks suggest a west-east younging trend of a scissor-like closure of the Mongol-Okhotsk ocean (Donskaya and others, 2008). While as to the southern belt the closure occurred in late Carboniferous and post-collision intrusive rocks mainly produced at 300 to 280 Ma in the western Central Asian Orogenic Belt, the closure was completed in the Permian-Triassic and post-collision intrusive rocks range in age from 270 to 120 Ma in the eastern Central Asian Orogenic Belt. Therefore, the Permian-Triassic (260-220 Ma) crustal growth revealed by detrital zircons of this study cannot be applied to the western Central Asian Orogenic Belt, whose Phanerozoic crustal growth is expected around Late Carboniferous.

The continental crust can grow by lateral accretion of arc complexes in subduction zones and vertical addition of underplates in crust-mantle interface (Rudnick, 1990). As described above, the eastern Central Asian Orogenic Belt formed by final closure of the Paleo-Asian ocean, leading to formation of the Solonker suture and collision of the North China craton and the Mongolian Plate and Siberian craton. The Permian-Triassic (260-220 Ma) crustal growth may be related to the subduction and closure of the Paleo-Asian ocean. This is supported by the presence of Permian-Triassic ophiolites and volcanic and intrusive rocks. The Solonker ophiolite is considered to indicate the final collision between the North China craton and the Siberian craton. A single Rb-Sr isochron age of ~262 Ma (Wang and Liu, 1986) for the Balengshan ophiolite (~10 km northwest of Linxi) has been reported from the Solonker suture zone. 299 to 292 Ma ages also have been determined by dating ophiolitic gabbros

(Jian and others, 2008). In addition, basaltic andesite and rhyolite in Xilinhot in central Inner Mongolia (situated in the Solonker suture zone) yield weighted mean $^{206}Pb/^{238}U$ ages of 281±3 Ma and 279±3 Ma, respectively (Zhang and others, 2008). The Xilinhot mafic rocks show an asthenospheric mantle-like component ($^{87}Sr/^{86}Sr(t) \approx 0.704$-$0.705$, $\varepsilon_{Nd}(t) \approx 6.87$-$7.90$, $(^{206}Pb/^{204}Pb)_i = 18.08$-$18.18$) (Zhang and others, 2008). These characteristics are consistent with the age of the arc granitoids (~310 Ma), which constrain timing of the final collision along the Solonker suture zone to be no earlier than 310 Ma (Chen and others, 2000, 2009). Based on geochronological and geochemical data in Inner Mongolia and southern Mongolia, Jian and others (2010) suggest that the subduction and collision along the Solonker suture occurred between 300 to 270 Ma and slab break-off at 255 to 248 Ma. Li and others (2007) reported a zircon U-Pb age of 239 ± 5 Ma for a muscovite granite from Linxi (east Xilinhot). They considered the rock to have formed as a result of Solonker suturing. Wu and others (2007) also suggested that suturing of the Solonker suture zone occurred at ~250 Ma based on geochemical and geochronological data for the Hulan Group on the eastern extension of the Solonker suture, which is younger than timing reported by Jian and others (2010). It is possible that the closure is disochronous, which is consistent with the younging trend as indicated by post-collision volcanic rocks. Further work is needed. Permian-Triassic volcanic and intrusive rocks in the age range from 290 to 210 Ma are widespread and can be classified into two groups: Permian (290-250 Ma) (Sun and others, 2000; Shi and others, 2004) and Late Triassic (230-210 Ma) (Wu and others, 2000, 2002, 2004; Chen and others, 2000, 2009; Wang and others, 2004; Ge and others, 2005; Liu and others, 2005; Xu and others, 2009). As discussed above, if the subduction and closure of the Paleo-Asian ocean occurred between 300 to 250 Ma according to previous studies, the 290 to 250 Ma and 230 to 210 Ma volcanic and intrusive rocks may represent lateral accretion of arc complexes in subduction zone and vertical addition of underplates in post-collision environment, respectively. They show typical characteristics of the Central Asian Orogenic Belt with slightly negative to positive ε_{Nd} (t) values (−2 to 5.60) and young Nd model age (1000-500 Ma) except for the granites in the Jiamusi Massif with negative ε_{Nd} (t) (−6.84 to −7.36) and relatively older model ages (~1600 Ma). These indicate the involvement of the Precambrian crust. The Xinglonggou Formation in this study represents the first sedimentation after the final collision of the Siberian Plate with the North China craton. The closure of the Paleo-Asian ocean led to mixed sources of the North China craton and the eastern Central Asian Orogenic Belt in Xinglonggou sandstones. 260 to 220 Ma Xinglonggou zircons can be interpreted by mixing of Permian-Triassic (260-220 Ma) new crustal additions with Precambrian crust. The subduction and closure of the Paleo-Asian ocean may have been responsible for this crustal growth.

Although the timing and mechanism of the amalgamation between the North China and Siberian Plate is controversial, many workers favor the Late Permian to early Triassic (ca. 300-230 Ma) amalgamation along the Solonker suture zone (Zhang and others, 1984; Wang and Liu, 1986; Wang and Mo, 1995; Yin and Nie, 1996; Davis and others, 2001; Xiao and others, 2003; Yang and others, 2006, Lin and others, 2008; Jian and others, 2010). Yang and others (2006) studied detrital zircons from Paleozoic to Late Mesozoic (304-143 Ma) strata in the Xishan area near Beijing. Their results show a significant change in source provenance in Late Triassic to Late Jurassic (205-158 Ma) sandstones, which contain a group of Phanerozoic zircons with positive ε_{Hf} (t) values, distinct from known igneous zircons in the North China craton. They suggest a source from the eastern Central Asian Orogenic Belt, resulting from the exhumation and denudation of rocks due to uplift of the eastern Central Asian Orogenic Belt. Together with these results, our study supports closure of the eastern Solonker suture zone at the end-Permian (~250 Ma). Since the Phanerozoic zircons from the North China craton are characterized by negative ε_{Hf} (t) values (Yang and others, 2006), the two youngest zircons with positive ε_{Hf} (t) values from the Xinglonggou sandstones constrain uplift of the eastern Central Asian Orogenic Belt to be no older than 208 Ma. This is also supported by an east-west-trending belt with numerous granitoid plutons ranging in age from 285 to 217 Ma along the northern margin of the North China craton (Ma and others, 2004; Zhang and others, 2004), which are considered to have resulted from collision between the North China craton and the Mongolian Plate (Wang and Liu, 1986; Wang and Mo, 1995).

As stated above, combination of Lu-Hf isotope and U-Pb age of detrital zircons from the Xinglonggou Formation revealed two episodes of crustal growth, one at Archean (ca. 2.5 Ga) in agreement with the North China craton and the other at 260 to 220 Ma related to the eastern Central Asian Orogenic Belt. As to the Archean crustal growth, it is consistent with the recent research on detrital zircons from modern rivers drained within the North China craton (Yang and others, 2009). In addition, the Archean peak agrees well with the worldwide compilations (for example, Pietranik and others, 2008; Condie and others, 2009). The Permian-Triassic (260-220 Ma) crustal growth is considered to be related to collision between the North China craton and the Mongolian Plate along the eastern Solonker suture, which records the termination of the Central Asian Orogenic Belt. The Solonker suture is 700 km long and 60 km wide and extends from Solonker via Sonid Yuoqi to Linxi in Inner Mongolia and further west and northeast (Xiao and others, 2003), which represents a large area of Permian-Triassic (260-220 Ma) crustal growth. However, worldwide compilations do not suggest significant crustal growth after 450 Ma (Condie, 1998, 2000; Condie and others, 2009). Although there are cases of classic orogenic belts considered to be significant Phanerozoic crustal growth based on positive ε_{Nd} (t) of granitoids just as in Central Asian Orogenic Belt, *in-situ* determinations of U-Pb ages, Hf and oxygen isotopes of detrital zircons from the Lachlan Fold Belt of southeastern Australia reveal no Phanerozoic zircons having a Hf isotopic composition that approaches that of the depleted mantle at time of crystallization, which means they were derived by re-melting, rather than juvenile, crustal rocks (Kemp and others, 2006; Hawkesworth and Kemp, 2006a, 2006b). However, the analysis of detrital zircons in this study indeed reveals Permian-Triassic (260-220 Ma) crustal growth with ε_{Hf} (t) close to depleted mantle values. This implies extensive juvenile crustal additions during this period. Although the amount and rate of the crustal growth can not be established according to our data, the Permian-Triassic (260-220 Ma) crustal growth is significant. The Triassic crustal growth has also been reported in the Canadian Cordillera deduced from geochemical characteristics of Late-Paleozoic and Triassic mantle-derived magma (Lapierre and others, 2003). Our study provides evidence for significant Permian-Triassic (260-220 Ma) crustal growth in the eastern Central Asian Orogenic Belt.

Why did such a large area of Permian-Triassic (260-220 Ma) crustal growth occur in the Central Asian Orogenic Belt? Previous studies suggest the relationship between supercontinent assembly and crustal growth (for example, Condie, 1998, 2000), and the Permian-Triassic corresponds to the assembly of Pangaea, but whether there is any relationship between them needs full discussion of supercontinent reconstruction, which is beyond the scope of this paper. If this is the result of assembly of Pangaea, why Permian-Triassic crustal growth is rare in other areas? If this is a particular event in the eastern Central Asian Orogenic Belt, is there any relationship between the growth and Mesozoic reactivation of the North China craton? All these need further studies.

CONCLUSIONS

In situ U-Pb ages and Hf isotopic data from detrital zircons in the Xinglonggou Formation, western Liaoning, provide important constraint on the source provenance and tectonic evolution of the eastern Central Asian Orogenic Belt. Zircons from the Xinglonggou sandstones are characterized by two major groups of U-Pb ages (2.6-2.4 Ga and 260-220 Ma) except for three grains (1.9-1.6 Ga). Hf isotopic compositions show juvenile crustal additions at 2.6 to 2.4 Ga and 260 to 220 Ma, while ancient crustal reworking occurred at 1.9 to 1.6 Ga.

Mixing of detritus from both the North China craton and the eastern Central Asian Orogenic Belt suggests that end-Permian (~250 Ma) closure of the Paleo-Asian ocean and collision between the North China craton and the Siberian Plate along the eastern Solonker zone. The youngest zircons constrain uplift of the eastern Central Asian Orogenic Belt to be no older than 208 Ma. Thus, the Permian-Triassic (260-220 Ma) crustal growth is related to the subduction of the Paleo-Asian ocean Plate. The analysis of detrital zircons in this study reveal significant Permian-Triassic (260-220 Ma) crustal growth with ε_{Hf} (t) close to depleted mantle values in the eastern Central Asian Orogenic Belt.

ACKNOWLEDGMENTS

This study is jointly supported by the MOST special funds from the State Key Laboratory of Continental Dynamics and the State Key Laboratory of Geological Processes and Mineral Resources, the National Nature Science Foundation of China (Grants 40973020, 40821061, 90714010 and 40673019), and the Ministry of Education of China (B07039). We thank J. J. Veevers and two anonymous reviewers for their helpful comments.

REFERENCES

Andersen, T., 2002, Correction of Common Lead in U-Pb Analyses that do not Report ^{204}Pb: Chemical Geology, v. 192, p. 59–79, doi: 10.1016/S0009-2541(02)00195-X.

Bichert-Toft, J., and Albarède, F., 1997, The Lu-Hf isotope geochemistry of chondrites and the evolution of the mantle-crust system: Earth and Planetary Science Letters, v. 148, p. 243–258, doi: 10.1016/S0012-821X(97)00040-X.

Buchan, C., Cunningham, D., Windley, B. F., and Tomurhuu, D., 2001, Structural and lithological characteristics of the Bayankhongor ophiolite zone, Central Mongolia: Journal of the Geological Society, London, v. 158, p. 445–460, doi: 10.1144/jgs.158.3.445.

Campbell, I. H., and Allen, C. M., 2008, Formation of supercontinents linked to increases in atmospheric oxygen: Nature Geoscience, v. 1, p. 554–558, doi: 10.1038/ngeo259.

Chen, B., and Arakawa, Y., 2005, Elemental and Nd-Sr isotopic geochemistry of granitoids from the West Junggar foldbelt (NW China), with implications for Phanerozoic continental growth: Geochimica et Cosmochimica Acta, v. 69, p. 1307–1320, doi: 10.1016/j.gca.2004.09.019.

Chen, B., and Jahn, B. M., 2004, Genesis of post-collisional granitoids and basement nature of the Junggar Terrane, NW China: Nd-Sr isotope and trace element evidence: Journal of Asian Earth Sciences, v. 23, p. 691–703, doi: 10.1016/S1367-9120(03)00118-4.

Chen, B., Jahn, B. M., Wilde, S., and Xu, B., 2000, Two contrasting Paleozoic magmatic belts in northern Inner Mongolia, China: petrogenesis and tectonic implications: Tectonophysics, v. 328, p. 157–182, doi: 10.1016/S0040-1951(00)00182-7.

Chen, B., Jahn, B. M., and Tian, W., 2009, Evolution of the Solonker suture zone: Constraints from zircon U-Pb ages, Hf isotopic ratios and whole-rock Nd-Sr isotope compositions of subduction and collision-related magmas and forearc sediments: Journal of Asian Earth Sciences, v. 34, p. 245–257, doi: 10.1016/j.jseaes.2008.05.007.

Chen, Y. X., Chen, W. J., Zhou, X. H., Li, Z. J., Liang, H. D., Li, Q., Xu, K., Fan, Q. C., Zhang, G. H., Wang, F., Wang, Y., Zhou, S. Q., Chen, S. H., Hu, B., and Wang, Q. J., 1997, Liaoxi and Adjacent Mesozoic Volcanic rocks: Chronology, Geochemistry and Tectonic Settings: Beijing, The Seismological Press, 22 p. (in Chinese).

Cheng, R. Y., Wu, F. Y., Ge, W. C., Sun, D. Y., Liu, X. M., and Yang, J. H., 2006, Emplacement age of the Raohe Complex in eastern Heilongjiang Province and the tectonic evolution of the eastern part of Northeastern China: Acta Petrologica Sinica, v. 22, p. 353–376 (in Chinese with English abstract).

Chu, N. C., Taylor, R. N., Chavagnac, V., Nesbitt, R. W., Boella, R. M., Milton, J. A., German, C. R., Bayon, G., and Burton, K., 2002, Hf isotope ratio analysis using multi-collector inductively coupled plasma mass spectrometry: an evaluation of isobaric interference corrections: Journal of Analytical Atomic Spectrometry, v. 17, p. 1567–1574, doi: 10.1039/b206707b.

Coleman, R. G., 1989, Continental growth of northwest China: Tectonics, v. 8, p. 621–635.

Condie, K. C., 1998, Episodic continental growth and supercontinents: a mantle avalanche connection: Earth and Planetary Science Letters, v. 163, p. 97–108, doi: 10.1016/S0012-821X(98)00178-2.

——— 2000, Episodic continental growth models: afterthoughts and extensions: Tectonophysics, v. 322, p. 153–162, doi: 10.1016/S0040-1951(00)00061-5.
Condie, K. C., Beyer, E., Belousova, E. A., Griffin, W. L., and O'Reilly, S. Y., 2005, U-Pb isotopic ages and Hf isotopic composition of single zircons: The search for juvenile Precambrian continental crust: Precambrian Research, v. 139, p. 42–100, doi: 10.1016/j.precamres.2005.04.006.
Condie, K. C., Belousova, E. A., Griffin, W. L., and Sircombe, K. N., 2009, Granitoid events in space and time: Constraints from igneous and detrital zircon age spectra: Gondwana Research, v. 15, p. 228–242, doi: 10.1016/j.gr.2008.06.001.
Coogan, L. A., and Hinton, R. W., 2006, Do the trace element compositions of detrital zircons require Hadean continental crust?: Geology, v. 34, p. 633–636, doi: 10.1130/G22737.1
Davis, G. A., Zheng, Y. D., Wang, C., Darby, B. J., Zhang, C. H., and Gehrels, G. E., 2001, Mesozoic tectonic evolution of the Yanshan fold and thrust belt, with emphasis on Hebei and Liaoning Provinces, northern China, *in* Hendrix, M. S., and Davis, G. A., editors, Paleozoic and Mesozoic Tectonic Evolution of Central Asia: From Continental Assembly to Intracontinental Deformation: Geological Society of America, Memoir, v. 194, p. 171–197, doi: 10.1130/0-8137-1194-0.171.
De Bievre, P., and Taylor, P. D. P., 1993, Table of the isotopic compositions of the elements: International Journal of Mass Spectrometry and Ion Processes, v. 123, p. 149–166, doi: 10.1016/0168-1176(93)87009-H.
Donskaya, T. V., Windley, B. F., Mazukabzov, A. M., Kröner, A., Sklyarov, E. V., Gladkochub, D. P., Ponomarchuk, V. A., Badarch, G., Reichow, M. K., and Hegner, E., 2008, Age and evolution of late Mesozoic metamorphic core complexes in southern Siberia and northern Mongolia: Journal of the Geological Society, London, v. 165, p. 405–421, doi: 10.1144/0016-76492006-162.
Fan, W. M., Guo, F., Wang, Y. J., and Lin, G., 2003, Late Mesozoic calc-alkaline volcanism of post-orogenic extension in the northern Da Hinggan Mountains, Northeastern China: Journal of Volcanology and Geothermal Research, v. 121, p. 115–135, doi: 10.1016/S0377-0273(02)00415-8.
Ferry, J. M., and Watson, E. B., 2007, New thermodynamic models and revised calibrations for the Ti-in-zircon and Zr-in-rutile thermometers: Contributions to Mineralogy and Petrology, v. 154, p. 429–437, doi: 10.1007/s00410-007-0201-0.
Gao, J., and Klemd, R., 2003, Formation of HP-LT rocks and their tectonic implications in the western Tianshan Orogen, NW China: geochemical and age constraints: Lithos, v. 66, p. 1–22, doi: 10.1016/S0024-4937(02)00153-6.
Gao, S., Rudnick, R. L., Yuan, H. L., Liu, X. M., Liu, Y. S., Xu, W. L., Ling, W. L., Ayers, J. C., Wang, X. C., and Wang, Q. H., 2004, Recycling lower continental crust in the North China craton: Nature, v. 432, p. 892–897, doi: 10.1038/nature03162.
Ge, W. C., Wu, F. Y., Zhou, C. Y., and Zhang, J. H., 2005, Zircon U-Pb ages and its significance of the Mesozoic granites in the Wulanhaote region, central Da Hinggan Mountain: Acta Petrologica Sinica, v. 21, p. 749–762 (in Chinese with English abstract).
Goldschmidt, V. M., 1933, Grundlagen der quantitativen Geochemie: Fortschritte der Mineralogic Kirstlographie Petrographie, v. 17, p. 112.
Griffin, W. L., Wang, X., Jackson, S. E., Pearson, N. J., O'Reilly, S. Y., Xu, X. S., and Zhou, X. M., 2002, Zircon chemistry and magma mixing, SE China: in-situ analysis of Hf isotopes, Tonglu and Pingtan igneous complexes: Lithos, v. 61, p. 237–269, doi: 10.1016/S0024-4937(02)00082-8.
Griffin, W. L., Belousova, E. A., Shee, S. R., Pearson, N. J., and O'Reilly, S. Y., 2004, Archean crustal evolution in the northern Yilgarn Craton: U-Pb and Hf-isotope evidence from detrital zircons: Precambrian Research, v. 131, p. 231–282, doi: 10.1016/j.precamres.2003.12.011.
Han, B. F., Wang, S. G., Jahn, B. M., Hong, D. W., Kagami, H., and Sun, Y. L., 1997, Depleted-mantle magma source for the Ulungur River A-type granites from North Xinjiang, China: geochemistry and Nd-Sr isotopic evidence, and implications for Phanerozoic crustal growth: Chemical Geology, v. 138, p. 135–159, doi: 10.1016/S0009-2541(97)00003-X.
Han, B. F., Kagami, H., and Li, H. M., 2004, Age and Nd-Sr isotopic geochemistry of the Guangtoushan alkaline granite, Hebei Province, China: implications for early Mesozoic crust-mantle interaction in North China Block: Acta Petrologica Sinica, v. 20, p. 1375–1388 (in Chinese with English abstract).
Han, B. F., Ji, J. Q., Song, B., Chen, L. H., and Zhang, L., 2006, Late Paleozoic vertical growth of continental crust around the Junggar Basin, Xinjiang, China: Acta Petrologica Sinica, v. 22, p. 1077–1086 (in Chinese with English abstract).
Hanchar, J. M., and Hoskin, P. W. O., 2003, Zircon: Reviews in Mineralogy and Geochemistry, v. 53, 500 p.
Hawkesworth, C. J., and Kemp, A. I. S., 2006a, Evolution of the continental crust: Nature, v. 443, p. 811–817, doi: 10.1038/nature05191.
——— 2006b, Using hafnium and oxygen isotopes in zircons to unravel the record of crustal evolution: Chemical Geology, v. 226, p. 144–162, doi: 10.1016/j.chemgeo.2005.09.018.
Hawkesworth, C. J., Dhuime, B., Pietranik, A. B., Cawood, P. A., Kemp, A. I. S., and Storey, C. D., 2010, The generation and evolution of the continental crust: Journal of the Geological Society, London, v. 167, p. 229–248, doi: 10.1144/0016-76492009-072.
Heinhorst, J., Lehmann, B., Ermolov, P., Serykh, V., and Zhurutin, S., 2000, Paleozoic crustal growth and metallogeny of Central Asia: evidence from magmatic-hydrothermal ore systems of Central Kazakhstan: Tectonophysics, v. 328, p. 69–87, doi: 10.1016/S0040-1951(00)00178-5.
Helo, C., Hegner, E., Kröner, A., Badarch, G., Tomurtogoo, O., Windley, B. F., and Dulski, P., 2006, Geochemical signature of Paleozoic accretionary complexes of the Central Asian Orogenic Belt in South Mongolia: Constraints on arc enviroments and crustal growth: Chemical Geology, v. 227, p. 236–257, doi: 10.1016/j.chemgeo.2005.10.003.
Hirata, T., and Nesbitt, R. W., 1995, U-Pb isotope geochronology of zircon: evaluation of the laser probe-inductively coupled plasma mass spectrometry technique: Geochimica et Cosmochimica Acta, v. 59, p. 2491–2500, doi: 10.1016/0016-7037(95)00144-1.

Hirata, T., Iizuka, T., and Orihashi, Y., 2005, Reduction of mercury background on ICP-mass spectrometry for *in situ* U-Pb age determinations of zircon samples: Journal of Analytical Atomic Spectrometry, v. 20, p. 696–701, doi: 10.1039/b504153h.
Hong, D. W., Huang, H. Z., Xiao, Y. J., Xu, H. M., and Jin, M. Y., 1995, Permian alkaline granites in central Inner Mongolia and their geodynamic significance: Acta Geologica Sinica, v. 8, p. 27–39, doi: 10.1111/j.1755-6724.1995.mp8001003.x.
Hong, D. W., Zhang, J. S., Wang, T., Wang, S. G., and Xie, X. L., 2004, Continental crustal growth and the supercontinental cycle: evidence from the Central Asian Orogenic Belt: Journal of Asian Earth Sciences, v. 23, p. 799–813, doi: 10.1016/S1367-9120(03)00134-2.
Hu, A. Q., Jahn, B. M., Zhang, G. X., Chen, Y. B., and Zhang, Q. F., 2000, Crustal evolution and Phanerozoic crustal growth in northern Xinjiang: Nd isotopic evidence: part I. Isotopic characterization of basement rocks: Tectonophysics, v. 328, p. 15–51, doi: 10.1016/S0040-1951(00)00176-1.
Hu, Z. C., and Gao, S., 2008, Upper Crustal Abundances of Trace Elements: A revision and update: Chemical Geology, v. 253, p. 205–221, doi: 10.1016/j.chemgeo.2008.05.010.
Iizuka, T., and Hirata, T., 2005, Improvements of precision and accuracy in in-situ Hf isotope microanalysis of zircon using the laser ablation-MC-ICPMS technique: Chemical Geology, v. 220, p. 121–137, doi: 10.1016/j.chemgeo.2005.03.010.
Iizuka, T., Hirata, T., Komiya, T., Rino, S., Katayama, I., Motoki, A., and Maruyama, S., 2005, U-Pb and Lu-Hf isotope systematics of zircons from the Mississippi River sand: Implications for reworking and growth of continental crust: Geology, v. 33, p. 485–488, doi: 10.1130/G21427.1.
Jackson, S. E., Pearson, N. J., Griffin, W. L., and Belousova, E. A., 2004, The application of laser ablation-inductively coupled plasma-mass spectrometry to in situ U-Pb zircon geochronology: Chemical Geology, v. 211, p. 47–69, doi: 10.1016/j.chemgeo.2004.06.017.
Jahn, B. M., 2004, The central Asian orogenic belt and growth of the continental crust in the Phanerozoic. Aspects of the Tectonic Evolution of China: Geological Society, London, Special Publication, v. 226, p. 73–100, doi: 10.1144/GSL.SP.2004.226.01.05.
Jahn, B. M., Wu, F. Y., and Chen, B., 2000a, Granitoids of the Central Asian Orogenic Belt and continental growth in the Phanerozoic: Transactions of the Royal Society of Edinburgh: Earth Sciences (GSA Special Publications), v. 91, p. 181–193, doi: 10.1130/0-8137-2350-7.181.
Jahn, B. M., Wu, F. Y., and Hong, D. W., 2000b, Important crustal growth in the Phanerozoic: Isotopic evidence of granitoids from east-central Asia: Proceeding of the Indian Academy of Science—Earth and Planetary Sciences (Journal of Earth System Science), v. 109, p. 5–20, doi: 10.1007/BF02719146.
Jahn, B. M., Wu, F. Y., Capdevila, R., Martineau, F., Zhao, Z. H., and Wang, Y. X., 2001, Highly evolved juvenile granites with tetrad REE patterns: the Woduhe and Baerzhe granites from the Great Xing'an Mountains in NE China: Lithos, v. 59, p. 171–198, doi: 10.1016/S0024-4937(01)00066-4.
Jahn, B. M., Capdevila, R., Liu, D. Y., Vernon, A., and Badarch, G., 2004, Sources of Phanerozoic granitoids in the transect Bayanhongor-Ulaan Baatar, Mongolia: geochemical and Nd isotopic evidence and implications for Phanerozoic crustal growth: Journal of Asian Earth Sciences, v. 23, p. 629–653, doi: 10.1016/S1367-9120(03)00125-1.
Jian, P., Liu, D. Y., Kröner, A., Windley, B. F., Shi, Y. R., Zhang, F. Q., Shi, G., Miao, L., Zhang, W., Zhang, Q., Zhang, L., and Ren, J., 2008, Time scale of an early to mid-Paleozoic orogenic cycle of the long lived Central Asian Orogenic Belt, Inner Mongolia of China: Implications for continental growth: Lithos, v. 101, p. 233–259, doi: 10.1016/j.lithos.2007.07.005.
Jian, P., Liu, D. Y., Kröner, A., Windley, B. F., Shi, Y. R., Zhang, W., Zhang, F. Q., Miao, L. C., Zhang, L. Q., and Tomurhuu, D., 2010, Evolution of a Permian intraoceanic arc-trench system in the Solonker suture zone, Central Asian Orogenic Belt, China and Mongolia: Lithos, v. 118, p. 169–190, doi: 10.1016/j.lithos.2010.04.014.
Kemp, A. I. S., Hawkesworth, C. J., Paterson, B. A., and Kinny, P. D., 2006, Episodic growth of the Gondwana supercontinent from hafnium and oxygen isotopes in zircon: Nature, v. 439, p. 580–583, doi: 10.1038/nature04505.
Khain, E. V., Bibokova, E. V., Kröner, A., Zhuravlev, D. Z., Sklyarov, E. V., Fedotova, A. A., and Kravchenko-Berezhnoy, I. R., 2002, The most ancient ophiolites of the Central Asian fold belt: U-Pb and Pb-Pb zircon ages for the Dunzhugur complex, Eastern Sayan, Siberia, and geodynamic implications: Earth and Planetary Science Letters, v. 199, p. 311–325, doi: 10.1016/S0012-821X(02)00587-3.
Kinnaird, J., and Bowden, P., 1987, African anorogenic alkaline magmatism and mineralization—a discussion with reference to the Niger-Nigerian province: Geological Journal, v, 22, p. 297–340, doi: 10.1002/gj.3350220622.
Kirkland, C. L., Strachan, R. A., and Prave, A. R., 2008, Detrital zircon signature of the Moine Supergroup, Scotland: Contrasts and comparisons with other Neoproterozoic successions within the circum-North Atlantic region: Precambrian Research, v. 163, p. 332–350, doi: 10.1016/j.precamres.2008.01.003.
Konopelko, D., Biske, G., Seltmann, R., Eklund, O., and Belyatsky, B., 2007, Hercynian post-collisional A-type granites of the Kokshaal Range, Southern Tien Shan, Kyrgyzstan: Lithos, v. 97, p. 140–160, doi: 10.1016/j.lithos.2006.12.005.
Kovalenko, V. I., Yarmolyuk, V. V., Kovach, V. P., Kotov, A. B., Salnikova, E. B., and Larin, A. M., 2004, Isotope provinces, mechanisms of generation and sources of the continental crust in the Central Asian mobile belt: Geological and isotopic evidence: Journal of Asian Earth Sciences, v. 23, p. 605–627, doi: 10.1016/S1367-9120(03)00130-5.
Kröner, A., Hegner, E., Lehmann, B., Heinhorst, J., Wingate, M. T. D., Liu, D. Y., and Ermelov, P., 2008, Palaeozoic arc magmatism in the Central Asian Orogenic Belt of Kazakhstan: SHRIMP zircon ages and whole-rock Nd isotopic systematics: Journal of Asian Earth Sciences, v. 32, p. 118–130, doi: 10.1016/j.jseaes.2007.10.013.

Lapierre, H., Bosch, D., Tardy, M., and Struik, L. C., 2003, Late Paleozoic and Triassic plume-derived magmas in the Canadian Cordillera played a key role in continental crust growth: Chemical Geology, v. 201, p. 55–89, doi: 10.1016/S0009-2541(03)00224-9.
Li, J. Y., Sun, G. H., Li, Y. P., Gao, L. M., and Wang, Y. B., 2007, Shuangjingzi middle Triassic syn-collisional crust-derived two-mica granite in the east Inner Mongolia and its constraint in timing on the collision between Siberian and Sino-Korean paleo-plates and beginning of intracontinental orogeny in the Yanshan area: Acta Petrologica Sinica, v. 23, p. 565–582.
Li, M., ms, 2010, Crustal growth and evolution of Northeastern China as revealed by U-Pb age and Hf isotopes of detrital zircons from modern rivers: China University of Geosciences, Ph. D. thesis (in Chinese with English abstract).
Li, Q. L., Chen, F. K., Guo, J. H., Li, H. X., Yang, Y. H., and Siebel, W., 2007, Zircon ages and Nd-Hf isotopic composition of the Zhaertai Group (Inner Mongolia): Evidence for early Proterozoic evolution of the northern North China Craton: Journal of Asian Earth Sciences, v. 30, p. 573–590, doi: 10.1016/j.jseaes.2007.01.006.
Li, Z. X., Wartho, J. A., Occhipinti, S., Zhang, C. L., Li, X. H., Wang, J., and Bao, C. M., 2007, Early history of the eastern Sibao Orogen (South China) during the assembly of Rodinia: New mica $^{40}Ar/^{39}Ar$ dating and SHRIMP U-Pb detrital zircon provenance constraints: Precambrian Research, v. 159, p. 79–94, doi: 10.1016/j.precamres.2007.05.003.
Lin, W., Faure, M., Nomade, S., Shang, Q. H., and Renne, P. R., 2008, Permian-Triassic amalgamation of Asia: Insights from Northeast China sutures and their place in the final collision of North China and Siberia: Comptes Rendus Geosciences, v. 340, p. 190–201, doi: 10.1016/j.crte.2007.10.008.
Liu, W., 2002, Fluid-rock interaction during subsolidus microtextural development of alkali granite as exemplified by the Saertielieke pluton, Ulungur of the northern Xinjiang, China: Chemical Geology, v. 182, p. 473–482, doi: 10.1016/S0009-2541(01)00333-3.
Liu, W., and Pan, X. F., 2006, Methane-rich fluid inclusions from ophiolitic dunite and post-collisional mafic-ultramafic intrusion: The mantle dynamics underneath the Palaeo-Asian Ocean through to the post-collisional period: Earth and Planetary Science Letters, v. 242, p. 286–301, doi: 10.1016/j.epsl.2005.11.059.
Liu, W., Siebel, W., Li, X. J., and Pan, X. F., 2005, Petrogenesis of the Linxi granitoids, northern Inner Mongolia of China: Constraints on basaltic underplating: Chemical Geology, v. 219, p. 5–35, doi: 10.1016/j.chemgeo.2005.01.013.
Liu, X. M., ms, 2004, Geochemical research on the Mesozoic crust-mantle interaction in the North China craton: Northwest University, Ph.D. thesis (in Chinese with English abstract).
Liu, X. M., Gao, S., Diwu, C. R., and Ling, W. L., 2008, Precambrian crustal growth of Yangtze Craton as revealed by detrital zircon studies: American Journal of Science, v. 308, p. 421–468, doi: 10.2475/04.2008.02.
Ludwig, K. R., 2003, ISOPLOT 3: A Geochronological Toolkit for Microsoft Excel: Berkeley, California, Berkeley Geochronology Centre Special Publication 4, 74 p.
Luo, Y., Sun, M., Zhao, G. C., Li, S. Z., Ayers, J. C., Xia, X. P., and Zhang, J. H., 2008, A comparison of U-Pb and Hf isotopic compositions of detrital zircons from the North and South Liaohe Groups: Constraints on the evolution of the Jiao-Liao-Ji Belt, North China Craton: Precambrian Research, v. 163, p. 279–306, doi: 10.1016/j.precamres.2008.01.002.
Luo, Z. K., Miao, L. C., Guan, K., Qiu, Y. S., Qiu, Y. M., McNaughton, N. J., and Groves, D. I., 2001, SHRIMP U-Pb zircon age of magmatic rock in Paishanlou gold mine district, Fuxin, Liaoning Province, China: Geochimica, v. 30, p. 483–490 (in Chinese with English abstract).
——— 2003, SHRIMP U-Pb zircon dating of the Dushan granitic batholith and related granite-porphyry dyke, eastern Hebei Province, China, and their geological significance: Geochimica, v. 32, p. 173–180 (in Chinese with English abstract).
Ma, F., Mu, Z. G., and Liu, Y. L., 2004, Geochronology and geologic significance of the Orbicular dioritic rocks in Luanping, Hebei Province: Geological Review, v. 50, p. 360–364 (in Chinese with English abstract).
McLennan, S. M., 2001, Relationships between the trace element composition of sedimentary rocks and upper continental crust: Geochemistry Geophysics Geosystems, v. 2, 1021, doi: 10.1029/2000GC000109.
Miao, L. C., Qiu, Y. S, McNaughton, N. J., Luo, Z. K., Groves, D. I., Zhai, Y., Fan, W. M., Zhai, M. G., and Guan, K., 2002, SHRIMP U-Pb zircon geochronology of granitoids from Dongping area, Hebei Province, China: constraints on tectonic evolution and geodynamic setting for gold metallogeny: Ore Geology Reviews, v. 19, p. 187–204, doi: 10.1016/S0169-1368(01)00041-5.
Miao, L. C., Qiu, Y., McNaughton, N. J., Fan, W. M., Groves, D. I., and Zhai, M. G., 2003, SHRIMP U-Pb Zircon Ages of Granitoids in the Wulashan Gold Deposit, Inner Mongolia, China: timing of mineralization and tectonic implications: International Geology Review, v. 45, p. 548–562, doi: 10.2747/0020-6814.45.6.548.
Miao, L. C., Fan, W. M., Zhang, F. Q., Liu, D. Y., Jian, P., Shi, G. H., Tao, H., and Shi, Y. R., 2004, Zircon SHRIMP geochronology of the Xinkailing-Kele complex in the northwestern Lesser Xing'an Range, and its geological implications: Chinese Science Bulletin, v. 49, p. 201–209, doi: 10.1360/03wd0316.
Miao, L. C., Fan, W. M., Liu, D. Y., Zhang, F. Q., Shi, Y. R., and Guo, F., 2008, Geochronology and geochemistry of the Hegenshan ophiolitic complex: Implications for late-stage tectonic evolution of the Inner Mongolia-Daxinganling Orogenic Belt, China: Journal of Asian Earth Sciences, v. 32, p. 348–370, doi: 10.1016/j.jseaes.2007.11.005.
Mossakovsky, A. A., Ruzhentsev, S. V., Samygin, S. G., and Kheraskova, T. N., 1994, Central Asian Fold Belt: geodynamic evolution and formational history: Geotectonics, v. 27, p. 445–474.

Nelson, D. R., 2001, An assessment of the determination of depositional ages for Precambrian clastic sedimentary rocks by U-Pb dating of detrital zircons: Sedimentary Geology, v. 141–142, p. 37–60, doi: 10.1016/S0037-0738(01)00067-7.

Nozaka, T., and Liu, Y., 2002, Petrology of the Hegenshan ophiolite and its implication for the tectonic evolution of northern China: Earth and Planetary Science Letters, v. 202, p. 89–104, doi: 10.1016/S0012-821X(02)00774-4.

Pelleter, E., Cheilletz, A., Gasquet, D., Mouttaqi, A., Annich, M., El Hakour, A., Deloule, E., and Féraude, G., 2007, Hydrothermal zircons: a tool for ion microprobe U-Pb dating of gold mineralization (Tamlalt-Menhouhou gold deposit—Morocco): Chemical Geology, v. 245, p. 135–161, doi: 10.1016/j.chemgeo.2007.07.026.

Pickett, D. A., and Saleeby, J. B., 1999, Nd, Sr, and Pb isotopic characteristics of Cretaceous intrusive rocks from deep levels of the Sierra Nevada batholith, Tehachapi Mountains, California: Contributions to Mineralogy and Petrology, v. 118, p. 198–215, doi: 10.1007/BF01052869.

Pietranik, A. B., Hawkesworth, C. J., Storey, C. D., Kemp, A. I. S., Sircombe, K. N., Whitehouse, M. J., and Bleeker, W., 2008, Episodic, mafic crust formation from 4.5 to 2.8 Ga: New evidence from detrital zircons, Slave craton, Canada: Geology, v. 36, p. 875–876, doi: 10.1130/G24861A.1.

Pietranik, A., Hawkesworth, C., Storey, C., and Kemp, T., 2009, Depleted mantle evolution and how it is recorded in zircon: Geochimica et Cosmochimica Acta, v. 73, p. A1028, doi: 10.1016/j.gca.2009.05.012.

Pirajno, F., Mao, J. W., Zhang, Z. C., Zhang, Z. H., and Chai, F. M., 2008, The association of mafic-ultramafic intrusions and A-type magmatism in the Tian Shan and Altay orogens, NW China: Implications for geodynamic evolution and potential for the discovery of new ore deposits: Journal of Asian Earth Sciences, v. 32, p. 165–183, doi: 10.1016/j.jseaes.2007.10.012.

Rudnick, R. L., 1990, Continental crust: Growing from below: Nature, v. 347, p. 711–712, doi: 10.1038/347711a0.

Rudnick, R. L., and Gao, S., 2003, Composition of the continental crust, *in* Rudnick, R. L., editor, The Crust: Treatise on Geochemistry, v. 3, p. 1–64, doi: 10.1016/B0-08-043751-6/03016-4.

Samson, S. D., McClelland, W. C., Patchett, P. J., Gehrels, G. E., and Anderson, R. G., 1989, Evidence from neodymium isotopes for mantle contributions to Phanerozoic crustal genesis in the Canadian Cordillera: Nature, v. 337, p. 705–709, doi: 10.1038/337705a0.

Scherer, E., Munker, C., and Mezger, K., 2001, Calibration of the lutetium-hafnium clock: Science, v. 293, p. 683–687, doi: 10.1126/science.1061372.

Sengör, A. M. C., and Natal'in, B. A., 1996, Paleotectonics of Asia: fragments of a synthesis, *in* Yin, A., and Harrison, T. M., editors, The Tectonic Evolution of Asia: Cambridge, Cambridge University Press, p. 486–640.

Sengör, A. M. C., Natal'in, B. A., and Burtman, V. S., 1993, Evolution of the Altaid tectonic collage and Paleozoic crustal growth in Eurasia: Nature, v. 364, p. 299–307, doi: 10.1038/364299a0.

Shao, J. A., 1991, Crustal Evolution in the Middle Part of the Northern Margin of the Sino-Korean Plate: Beijing, Peking University Publishing House (in Chinese).

Shao, J. A., Han, Q. J., Zhang, L. Q., Mu, B. L., and Qiao, G. S., 1999, Two kinds of vertical accretion of the continental crust: an example of the Da Hinggan Mts: Acta Petrologica Sinica, v. 15, p. 600–606.

Shi, G. H., Miao, L. C., Zhang, F. Q., Jian, P., Fan, W. M., and Liu, D. Y., 2004, Emplacement age and tectonic implications of the Xilinhot A-type granite in Inner Mongolia. China: Chinese Science Bulletin, v. 49, p. 384–389 (in Chinese with English abstract), doi: 10.1007/BF03184272.

Storey, C. D., Jeffries, T. E., and Smith, M., 2006, Common lead-corrected laser ablation ICP-MS U-Pb systematics and geochronology of titanite: Chemical Geology, v. 227, doi: 10.1016/j.chemgeo.2005.09.003.

Sun, D. Y., Wu, F. Y., Li, H. M., and Lin, Q., 2000, Emplacement age of the postorogenic A-type granites in Northwestern Lesser Xing'an Ranges, and its relationship to the eastward extension of Suolunshan-Hegenshan-Zhalaite collisional suture zone: Chinese Science Bulletin, v. 45, p. 2217–2222 (in Chinese with English abstract), doi: 10.1007/BF03183282.

Sun, M., Yuan, C., Xiao, W. J., Long, X. P., Xia, X. P., Zhao, G. C., Lin, S. F., Wu, F. Y., and Kröner, A., 2008, Zircon U-Pb and Hf isotopic study of gneissic rocks from the Chinese Altai: Progressive accretionary history in the early to middle Palaeozoic: Chemical Geology, v. 247, p. 352–383, doi: 10.1016/j.chemgeo.2007.10.026.

Tang, K. D., 1990, Tectonic development of Paleozoic foldbelts at the north margin of the Sino-Korean craton: Tectonics, v. 9, p. 249–260, doi: 10.1029/TC009i002p00249.

Taylor, S. R., and McLennan, S. M., 1985, The Continental Crust: Its Composition and Evolution: Oxford, Blackwell Scientific Publication, 311 p.

——— 1995, The geochemical evolution of the continental crust: Reviews of Geophysics, v. 33, p. 241–265.

Taylor, S. R., McLennan, S. M., and McCulloch, M. T., 1983, Geochemistry of loess, continental crustal composition and crustal model ages: Geochimica et Cosmochimica Acta, v. 47, p. 1897–1905, doi: 10.1016/0016-7037(83)90206-5.

Tian, W., Chen, B., Liu, C. Q., and Zhang, H. F., 2007, Zircon U-Pb age and Hf isotopic composition of the Xiaozhangjiakou ultramafic pluton in northern Hebei: Acta Petrologica Sinica, v. 23, p. 583–590 (in Chinese with English abstract).

Tong, Y., Wang, T., Kovach, V. P., Hong, D. W., and Han, B. F., 2006, Age and origin of the Takeshiken postorogenic alkali-rich intrusive rocks in southern Altai, near the Mongolian border in China and its implication for continental growth: Acta Petrologica Sinica, v. 22, p. 1267–1278 (in Chinese with English abstract).

Veevers, J. J., Saeed, A., Belousova, E. A., and Griffin, W. L., 2005, U-Pb ages and source composition by Hf-isotope and trace-element analysis of detrital zircons in Permian sandstone and modern sand from southwestern Australia and a review of the paleogeographical and denudational history of the Yilgarn Craton: Earth Science Reviews, v. 68, p. 245–279, doi: 10.1016/j.earscirev.2004.05.005.

Vermeesch, P., 2004, How many grains are needed for a provenance study?: Earth and Planetary Science Letters, v. 224, p. 441–451, doi: 10.1016/j.epsl.2004.05.037.

Vervoort, J. D., and Patchett, P. J., 1996, Behavior of hafnium and neodymium isotopes in the crust: constraints from Precambrian crustally derived granites: Geochimica et Cosmochimica Acta, v. 60, p. 3717–3733, doi: 10.1016/0016-7037(96)00201-3.

Wan, Y. S., Liu, D. Y., Yin, X. Y., Wilde, S. A., Yang, Y. H., Zhao, H. Y., and Wu, J. S., 2007, SHRIMP geochronology and Hf isotope composition of zircons from the Tiejiashan granite and supercrustal rocks in the Anshan area, Liaoning province: Acta Petrologica Sinica, v. 23, p. 241–252 (in Chinese with English abstract).

Wang, H. Z., and Mo, X. X., 1995, An outline of the tectonic evolution of China: Episodes, v. 18, p. 6–16.

Wang, Q., and Liu, X. Y., 1986, Paleoplate tectonics between Cathaysia and Angaraland in Inner Mongolia of China: Tectonics, v. 5, p. 1073–1088, doi: 10.1029/TC005i007p01073.

Wang, T., Hong, D. W., Tong, Y., Han, B. F., and Shi, Y. R., 2005, Zircon U-Pb SHRIMP age and Origin of Post orogenic Lamazhao granitic pluton from Altai orogen: its implications for vertical continental growth: Acta Petrologica Sinica, v. 21, p. 640–650.

Wang, T., Jahn, B. M., Kovach, V. P., Tong, Y., Hong, D. W., and Han, B. F., 2009, Nd-Sr isotopic mapping of the Chinese Altai and implications for continental growth in the Central Asian Orogenic Belt: Lithos, v. 110, p. 359–372, doi: 10.1016/j.lithos.2009.02.001.

Wang, T., Zheng, Y. D., Li, T. B., and Gao, Y. J., 2004, Mesozoic granitic magmatism in extensional tectonics near the Mongolian border in China and its implications for crustal growth: Journal of Asian Earth Sciences, v. 23, p. 715–729, doi: 10.1016/S1367-9120(03)00133-0.

Watson, E. B., and Harrison, T. M., 2005, Zircon thermometer reveals minimum melting conditions on earliest Earth: Science, v. 308, p. 841–844, doi: 10.1126/science.1110873.

Watson, E. B., Wark, D. A., and Thomas, J. B., 2006, Crystallization thermometers for zircon and rutile: Contributions to Mineralogy and Petrology, v. 151, p. 413–433, doi: 10.1007/s00410-006-0068-5.

Weislogel, A. L., Graham, S. A., Chang, E. Z., Wooden, J. L., Gehrels, G. E., and Yang, H., 2006, Detrital zircon provenance of the Late Triassic Songpan-Ganzi complex: Sedimentary record of collision of the North and South China blocks: Geology, v. 34, p. 97–100, doi: 10.1130/G21929.1.

Whalen, J. B., Jenner, G. A., Longstaffe, F. J., Robert, F., and Gariepy, C., 1996, Geochemical and isotopic (O, Nd, Pb and Sr) constraints on A-type granite petrogenesis based on the Topsails igneous suite, Newfoundland Appalachians: Journal of Petrology, v. 37, p. 1463–1489, doi: 10.1093/petrology/37.6.1463.

Wilde, S. A., Dorsett-Bain, H. L., and Liu, J. L., 1997, The identification of a Late Pan-African granulite facies event in Northeastern China: SHRIMP U-Pb zircon dating of the Mashan Group at Liu Mao, Heilongjiang Province, China: Proceedings of the 30th International Geological Congress: Precambrian Geology and Metamorphic Petrology, v. 17, Part 1, p. 59–74.

Wilde, S. A., Zhang, X. Z., and Wu, F. Y., 2000, Extension of a newly identified 500 Ma metamorphic terrain in North East China: further U-Pb SHRIMP dating of the Mashan Complex, Heilongjiang Province, China: Tectonophysics, v. 328, p. 115–130, doi: 10.1016/S0040-1951(00)00180-3.

Windley, B. F., Alexeiev, D., Xiao, W. J., Kröner, A., and Badarch, G., 2007, Tectonic model for accretion of the Central Asian Orogenic Belt: Journal of the Geological Society, London, v. 164, p. 31–47, doi: 10.1144/0016-76492006-022.

Wu, F. Y., Jahn, B. M., Wilde, S. A., Lo, C. H., Yui, T. F., Lin, Q., Ge, W. C., and Sun, D. Y., 2003a, Highly fractionated I-type granites in NE China (I): geochronology and petrogenesis: Lithos, v. 66, p. 241–273, doi: 10.1016/S0024-4937(02)00222-0.

——— 2003b, Highly fractionated I-type granites in NE China (II): isotopic geochemistry and implications for crustal growth in the Phanerozoic: Lithos, v. 67, p. 191–204, doi: 10.1016/S0024-4937(03)00015-X.

Wu, F. Y., Jahn, B. M., Wilde, S. A., and Sun, D. Y., 2000, Phanerozoic crustal growth: U-Pb and Sr-Nd isotopic evidence from the granites in northeastern China: Tectonophysics, v. 328, p. 89–113, doi: 10.1016/S0040-1951(00)00179-7.

Wu, F. Y., Sun, D. Y., Li, H., Jahn, B. M., and Wilde, S. A., 2002, A-type granites in northeastern China: Age and geochemical constraints on their petrogenesis: Chemical Geology, v. 187, p. 143–173, doi: 10.1016/S0009-2541(02)00018-9.

Wu, F. Y., Wilde, S. A., Zhang, G. L., and Sun, D. Y., 2004, Geochronology and petrogenesis of the post-orogenic Cu-Ni sulfide-bearing mafic-ultramafic complexes in Jilin Province, NE China: Journal of Asian Earth Sciences, v. 23, p. 781–797, doi: 10.1016/S1367-9120(03)00114-7.

Wu, F. Y., Lin, J. Q., Wilde, S. A., Zhang, X. O., and Yang, J. H., 2005a, Nature and significance of the Early Cretaceous giant igneous event in eastern China: Earth and Planetary Science Letters, v. 233, p. 103–119, doi: 10.1016/j.epsl.2005.02.019.

Wu, F. Y., Yang, J. H., Liu, X. M., Li, T. S., Xie, L. W., and Yang, Y. H., 2005b, Hf isotopes of the 3.8 Ga zircons in eastern Hebei Province, China: Implications for early crustal evolution of the North China Craton: Chinese Science Bulletin, v. 50, p. 2473–2480, doi: 10.1360/982005-629.

Wu, F. Y., Yang, J. H., Wilde, S. A., and Zhang, X. O., 2005c, Geochronology, petrogenesis and tectonic implications of Jurassic granites in the Liaodong Peninsula, NE China: Chemical Geology, v. 221, p. 127–156, doi: 10.1016/j.chemgeo.2005.04.010.

Wu, F. Y., Yang, J. H., Zhang, Y. B., and Liu, X. M., 2006, Emplacement ages of the Mesozoic granites in southeastern part of the Western Liaoning Province: Acta Petrologica Sinica, v. 22, p. 315–325.

Wu, F. Y., Zhao, G. C., Sun, D. Y., Wilde, S. A., and Yang, J. H., 2007, The Hulan Group: Its role in the evolution of the Central Asian Orogenic Belt of NE China: Journal of Asian Earth Sciences, v. 30, p. 542–556, doi: 10.1016/j.jseaes.2007.01.003.

Wu, F. Y., Zhang, Y. B., Yang, J. H., Xie, L. W., and Yang, Y. H., 2008, Zircon U-Pb and Hf isotopic constraints on the Early Archean crustal evolution in Anshan of the North China Craton: Precambrian Research, v. 167, p. 339–362, doi: 10.1016/j.precamres.2008.10.002.

Xia, L. Q., Xia, Z. C., Xu, X. Y., Li, X. M., Ma, Z. P., and Wang, L. S., 2004, Carboniferous Tianshan igneous megaprovince and mantle plume: Geological Bulletin of China, v. 23, p. 903–910.

Xiao, W. J., Windley, B. F., Hao, J., and Zhai, M. G., 2003, Accretion leading to collision and the Permian Solonker suture, Inner Mongolia, China: Termination of the central Asian orogenic belt: Tectonics, v. 22, 1069. doi: 10.1029/2002TC001484.

Xu, B., and Chen, B., 1997, The structure and evolution of a Middle Paleozoic orogenic belt between the north China and Siberian blocks, northern Inner Mongolia, China: Science in China (Series D), v. 27, p. 227–232 (in Chinese with English abstract).

Xu, W. L., Ji, W. Q., Pei, F. P., Meng, E., Yu, Y., Yang, D. B., and Zhang, X. Z., 2009, Triassic volcanism in eastern Heilongjiang and Jilin provinces, NE China: Chronology, geochemistry, and tectonic implications: Journal of Asian Earth Sciences, v. 34, p. 392–402, doi: 10.1016/j.jseaes.2008.07.001.

Xu, X. Y., Li, X. M., Ma, Z. P., Xia, L. Q., Xia, Z. C., and Peng, S. X., 2006, LA-ICPMS zircon U-Pb dating of gabbro from the Bayingou ophiolite in the northern Tianshan Mountains: Acta Geologica Sinica, v. 80, p. 1168–1176.

Yakubchuk, A. S., 2002, The Baikalide-Altaid, Transbaikal-Mongolian and North Pacific orogenic collage: similarity and diversity of structural patterns and metallogenic zoning, *in* Blundell, D. J., Neubauer, F., and von Quadt, A., editors, The Timing and Location of Major Ore Deposits in an Evolving Orogen: Geological Society, London, Special Publication, v. 204, p. 273–297, doi: 10.1144/GSL.SP.2002.204.01.16.

Yakubchuk, A. S., Seltmann, R., Shatov, V., and Cole, A., 2001, The Altaids: tectonic evolution and metallogeny: Society of Economic Geologists Newsletter, v. 46, p. 7–14.

Yan, Y., Lin, G., Xia, B., Li, Z., Cui, X. J., and Yuan, G. B., 2006, U-Pb dating of single detrital zircon grains from Mesozoic sandstone in the Beipiao Basin in the eastern Yan-Liao Orogenic Belt, China: provenance and correlation of tectonic evolution: Journal of Asian Earth Sciences, v. 26, p. 669–681, doi: 10.1016/j.jseaes.2005.01.002.

Yang, J., Gao, S., Chen, C., Tang, Y. Y., Yuan, H. L., Gong, H. J., Xie, S. W., and Wang, J. Q., 2009, Episodic crustal growth of North China as revealed by U-Pb age and Hf isotopes of detrital zircons from modern rivers: Geochimica et Cosmochimica Acta, v. 73, p. 2660–2673, doi: 10.1016/j.gca.2009.02.007.

Yang, J. H., Wu, F. Y., Liu, X. M., and Xie, L. W., 2005, Zircon U-Pb ages and Hf isotopes and their geological significance of the Miyun rapakivi granites from Beijing, China: Acta Petrologica Sinica, v. 21, p. 1633–1644.

Yang, J. H., Wu, F. Y., Shao, J. A., Wilde, S. A., Xie, L. W., and Liu, X. M., 2006, Constraints on the timing of uplift of the Yanshan Fold and Thrust Belt, North China: Earth and Planetary Science Letters, v. 246, p. 336–352, doi: 10.1016/j.epsl.2006.04.029.

Yang, J. H., Wu, F. Y., Wilde, S. A., and Liu, X. M., 2007, Petrogenesis of Late Triassic granitoids and their enclaves with implications for post-collisional lithospheric thinning of the Liaodong Peninsula, North China Craton: Chemical Geology, v. 242, p. 155–175, doi: 10.1016/j.chemgeo.2007.03.007.

Yang, J. H., Wu, F. Y., Wilde, S. A., Belousova, E. A., and Griffin, W. L., 2008, Mesozoic decratonization of the North China block: Geology, v. 36, p. 467–470, doi: 10.1130/G24518A.1.

Yang, W., and Li, S. G., 2008, Geochronology and geochemistry of the Mesozoic volcanic rocks in Western Liaoning: Implications for lithospheric thinning of the North China Craton: Lithos, v, 102, p. 88–117, doi: 10.1016/j.lithos.2007.09.018.

Yin, A., and Nie, S., 1996, A Phanerozoic palinspastic reconstruction of China and its neighboring regions, *in* Yin, A., and Harrison T. M., editors, The Tectonic Evolution of Asia: Cambridge, Cambridge University Press, p. 442–485.

Yuan, H. L., Gao, S., Liu, X. M., Li, H. M., Günther, D., and Wu, F. Y., 2004, Accurate U-Pb Age and Trace Element Determinations of Zircon by Laser Ablation-Inductively Coupled Plasma Mass Spectrometry: Geostandards Newsletter, v. 28, p. 353–370, doi: 10.1111/j.1751-908X.2004.tb00755.x.

Yuan, H. L., Gao, S., Dai, M. N., Zong, C. L., Günther, D., Fontaine, G. H., Liu, X. M., and Diwu, C. R., 2008, Simultaneous determinations of U-Pb age, Hf isotopes and trace element compositions of zircon by excimer laser-ablation quadrupole and multiple-collector ICP-MS: Chemical Geology, v. 247, p. 100–118, doi: 10.1016/j.chemgeo.2007.10.003.

Zhang, S. H., Zhao, Y., Song, B., and Wu, H., 2004, The late Paleozoic gneissic granodiorite pluton in early Precambrian high-grade metamorphic terrains near Longhua county in northern Hebei Province, North China: result from zircon SHRIMP U-Pb dating and its tectonic implications: Acta Petrologica Sinica, v. 20, p. 621–626 (in Chinese with English abstract).

Zhang, S. H., Zhao, Y., Song, B., Yang, Z. Y., Hu, J. M., and Wu, H., 2007a, Carboniferous granitic plutons from the northern margin of the North China block: implications for a Late Paleozoic active continental margin: Journal of the Geological Society, London, v. 164, p. 451–463, doi: 10.1144/0016-76492005-190.

Zhang, S. H., Zhao, Y., Song, B., and Yang, Y. H., 2007b, Zircon SHRIMP U-Pb and in-situ Lu-Hf isotope analyses of a tuff from Western Beijing: evidence for missing late Paleozoic arc volcano eruptions at the northern margin of the North China block: Gondwana Research, v. 12, p. 157–165, doi: 10.1016/j.gr.2006.08.001.

Zhang, S. H., Zhao, Y., Song, B., Hu, J. M., Liu, S. W., Yang, Y. H., Chen, F. K., Liu, X. M., and Liu, J., 2009a, Contrasting Late Carboniferous and Late Permian-Middle Triassic intrusive suites from the northern margin of the North China craton: Geochronology, petrogenesis and tectonic implications: Geological Society of America Bulletin, v. 121, p. 181–200, doi: 10.1130/B26157.1.

Zhang, S. H., Zhao, Y., Liu, X. C., Liu, D. Y., Chen, F. K., Xie, L. W., and Chen, H. H., 2009b, Late Paleozoic to Early Mesozoic mafic-ultramafic complexes from the northern North China Block: Constraints on the composition and evolution of the lithospheric mantle: Lithos, v. 110, p. 229–246, doi: 10.1016/j.lithos.2009.01.008.

Zhang, X. H., Zhang, H. F., Tang, Y. J., Wilde, S. A., and Hu, Z. C., 2008, Geochemistry of Permian bimodal volcanic rocks from central Inner Mongolia, North China: Implication for tectonic setting and Phanerozoic continental growth in Central Asian Orogenic Belt: Chemical Geology, v. 249, p. 262–281, doi: 10.1016/j.chemgeo.2008.01.005.

Zhang, Z. M., Liu, J. G., and Coleman, R. G., 1984, An outline of the plate tectonics of China: Geological Society of America Bulletin, v. 95, p. 295–312, doi: 10.1130/0016-7606(1984)95<295:AOOTPT>2.0.CO;2.

Zhao, G. C., Wilde, S. A., Cawood, P. A., and Sun, M., 2001, Archean blocks and their boundaries in the North China Craton: lithological, geochemical, structural and P-T path constraints and tectonic evolution: Precambrian Research, v. 107, p. 45–73, doi: 10.1016/S0301-9268(00)00154-6.

Zhao, Z. H., Wang, Z. G., Zou, T. R., and Masuda, A., 1996, Study on petrogenesis of alkali-rich intrusive rocks of Ulungur, Xinjiang: Geochimica, v. 25, p. 205–220 (in Chinese with English abstract).

Zhao, Z. H., Xiong, X. L., Wang, Q., Wyman, D. A., Bao, Z. W., Bai, Z. H., and Qiao, Y. L., 2008, Underplating-related adakites in Xinjiang Tianshan, China: Lithos, v. 102, p. 374–391, doi: 10.1016/j.lithos.2007.06.008.

Zheng, J. P., Griffin, W. L., O'Reilly, S. Y., Lu, F. X., Yu, C. M., Zhang, M., and Li, H. M., 2004, U-Pb and Hf-isotope analysis of zircons in mafic xenoliths from Fuxian kimberlites: evolution of the lower crust beneath the North China craton: Contributions to Mineralogy and Petrology, v. 148, p. 79–103, doi: 10.1007/s00410-004-0587-x.

Zhou, C. Y., Wu, F. Y., Ge, W. C., Sun, D. Y., Abdel Rahman, A. A., Zhang, J. H., and Cheng, R. Y., 2005, Age, geochemistry and petrogenesis of the cumulate gabbro in Tahe, northern Da Hinggan Mountain: Acta Petrologica Sinica, v. 21, p. 763–775 (in Chinese with English abstract).

Zhou, M. F., Lesher, C. M., Yang, Z. Y., Li, J. W., and Sun, M., 2004, Geochemistry and petrogenesis of 270 Ma Ni-Cu-(PGE) sulfide bearing mafic intrusions in the Huangshan district, Eastern Xinjiang, Northwest China: implications for the tectonic evolution of the Central Asian orogenic belt: Chemical Geology, v. 209, p. 233–257, doi: 10.1016/j.chemgeo.2004.05.005.

Zhou, T. F., Yuan, F., Fan, Y., Zhang, D. Y., Cooke, D., and Zhao, G. C., 2008, Granites in the Sawuer region of the west Junggar, Xinjiang Province, China: Geochronological and geochemical characteristics and their geodynamic significance: Lithos, v. 106, p. 191–206, doi: 10.1016/j.lithos.2008.06.014.

Zhu, Y. F., Zhang, L. F., Gu, L. B., Guo, X., and Zhou, J., 2005, The zircon SHRIMP chronology and trace element geochemistry of the Carboniferous volcanic rocks in western Tianshan Mountains: Chinese Science Bulletin, v. 50, p. 2210–2212, doi: 10.1007/BF03182672.

Zonenshain, L. P., Kusmin, M. I., and Natapov, L. M., 1990, Mongol-Okhotsk Foldbelt, *in* Page, B. M., editor, Geology of the USSR: a plate-tectonic synthesis: Washington, D. C., American Geophysical Union, Geodynamic Series, v. 21, p. 97–120.